IDA

INSTITUTE FOR DEFENSE ANALYSES

Assessment of Thermal Neutron Activation Applied to Surface and Near Surface Unexploded Ordnance

Lisa Porter
David A. Sparrow

December 1997

Approved for public release;
distribution unlimited.

IDA Paper P-3339
Log: H 97-002000

DTIC QUALITY INSPECTED 4

19980310 177

This work was conducted under contract DASW01 94 C 0054, Task T-AM2-1528, for the Office of the Deputy Under Secretary of Defense, Environmental Security and Technology. The publication of this IDA document does not indicate endorsement by the Department of Defense, nor should the contents be construed as reflecting the official position of that Agency.

© 1997, 1998 Institute for Defense Analyses, 1801 N. Beauregard Street, Alexandria, Virginia 22311-1772 • (703) 845-2000.

This material may be reproduced by or for the U.S. Government pursuant to the copyright license under the clause at DFARS 252.227-7013 (10/88).

INSTITUTE FOR DEFENSE ANALYSES

IDA Paper P-3339

Assessment of Thermal Neutron Activation Applied to Surface and Near Surface Unexploded Ordnance

Lisa Porter
David A. Sparrow

PREFACE

This paper was prepared for the Assistant Deputy Under Secretary of Defense (Acquisition and Technology) for Environmental Security under a task entitled "Assessment of Traditional and Emerging Approaches to the Detection and Identification of Surface and Buried Unexploded Ordnance." This paper fulfills subtask (e) of that task.

We would like to thank our reviewers: Dr. James Silk, Dr. Michael Burlein, Dr. Jeff Schweitzer, and Dr. Robert Moler. Their comments and suggestions greatly improved the quality of this paper.

CONTENTS

FIGURES

TABLES

EXECUTIVE SUMMARY

A. BACKGROUND AND SCOPE

The Environmental Security Technology Certification Program (ESTCP) has invested in the development and demonstration of a number of technologies aimed at improving remediation of ordnance-contaminated sites. In one of these projects, ESTCP provided funds to Night Vision and Electronic Sensors Directorate (NVESD) for the Remote Controlled Surface/Near Surface UXO detection system. This system includes a remote-controlled vehicle, a Scheibel electromagnetic induction sensor for rapid search of large areas, and a thermal neutron activation (TNA) sensor for confirmation of energetic material associated with the metal detected by the induction sensor.

The advantage of the TNA sensor over traditional UXO sensors is that it responds to concentrations of nitrogen, which are very rare naturally, but very good as signatures of energetic materials. Most UXO systems use a detection scheme which responds to the metal casings associated with ordnance. The TNA sensor attempts to detect the presence of the explosive itself. This paper focuses on the performance of TNA in its confirmation role only, because TNA itself is too slow for large area searches.

B. THERMAL NEUTRON ACTIVATION

Thermal neutron activation is a technique for identifying the presence of particular nuclear isotopes in a sample of material. The sample is bathed with very low energy or "thermal" neutrons, which are captured at various rates by the atomic nuclei which are present. In most cases this capture process results in a gamma ray. The spectrum of gamma rays that emerge is unique for each species of atomic nucleus. Therefore, in principle, the composition of material can be determined by irradiating it with neutrons and measuring the resulting gamma ray spectra.

The approach is limited by both hardware and background issues. The detection systems have finite energy resolution, and further only detect a fraction of the γ rays that transit. The finite resolution means that the characteristic peaks from different atomic nuclei will overlap. Any attempt to detect small quantities of a material in the presence of many

other nuclear species will lead to an essentially smooth overall spectrum with few distinguishing features readily tied to any of the component species. This problem is directly related to the background issue—to identify and estimate the amounts of small quantities that may be present, the backgrounds from the more common materials must be determined and subtracted off. The low overall detection efficiency makes the background subtraction and target identification more difficult because of statistical fluctuations in the number of counts observed.

C. SYSTEM DEMONSTRATIONS

The TNA sensor system developed in this program was based on earlier work at Science Applications International Corporation (SAIC) for explosive detection in airport luggage searches and in countermine applications. This system uses a Cf-252 source to provide the neutrons. The photons are detected by NaI detectors in a ring around the source. At Socorro, 8 detectors were used, with counting times up to 5 minutes; at Yuma, 12 detectors were used, with counting times up to 10 minutes.

The TNA system was tested at Socorro, New Mexico, and Yuma, Arizona. The contractor provided data that yield the following results for their thresholds.

	P_d	P_{FA}	Threshold (cts/min)
Socorro	.54	.15	2.85
Yuma	.72	.22	1.5

These numbers correspond to a signal-to-noise ratio of order unity.

Figure ES-1 shows the performance curves calculated from this data.

These results may be viewed as a proof of concept, but the detection probabilities are too low and the false alarm rates are too high for useful application. The data allow some quantitative insight into what limits detection, as well as predictions about the performance to be expected as a result of possible hardware upgrades.

1. Limitations on Current Performance

There are two noise sources for this system. The first is the statistical error associated with finite counting times, proportional to the square root of the background counts. The second source is estimated by looking at the excess standard deviation (above what would be predicted from counting statistics) when the system measures the response

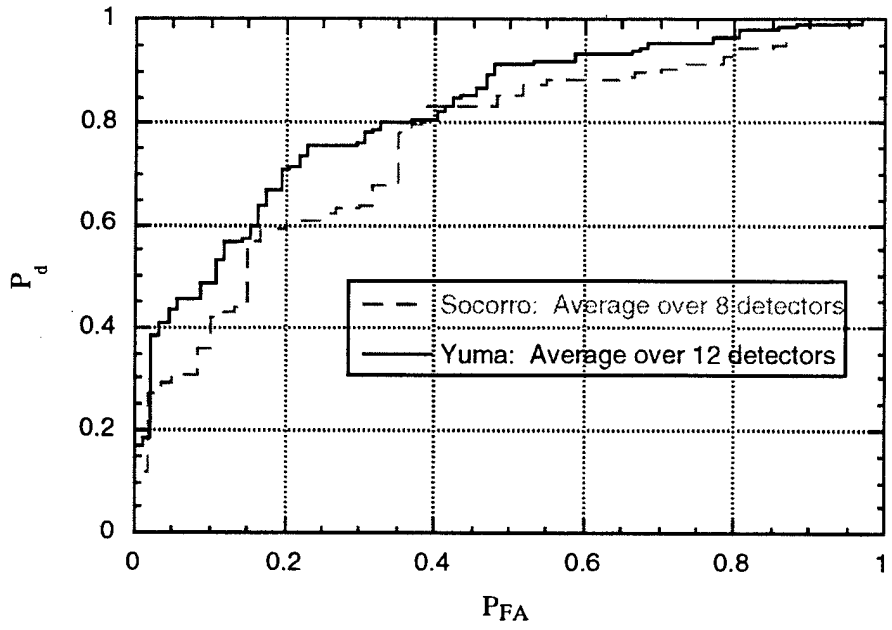

Figure ES-1. ROC Curves of Performance at Yuma and Socorro

at a number of sites with no ordnance. This second source then is "everything else." This additional error is referred to as "systematic" by SAIC, presumably because it includes many errors associated with the electronics. However, this error source is believed to be dominated by differences between the true background count rate and the modeled background rate. If so, this error is also "noise-like" because it is caused by variations in soil response around the "average" response determined by the model. Because this error source is also noise-like, it should add in quadrature with the contribution from the counting statistics. That the total error is about 1.5 times what would be expected from the counting statistics implies that the statistical and the "systematic" errors are comparable in size, with the contribution from the counting statistics being slightly smaller.

Signal strengths are limited by two mechanisms. First, for buried ordnance there is significant attenuation of the neutrons and, to a lesser extent, the photons through the soil. In addition, for the larger ordnance items the N14(n,p) reaction scavenges neutrons that would otherwise yield useful signal. Figure ES-2 shows the results of a semi-empirical model developed to predict what count rates per detector should be expected as a function of depth and ordnance nitrogen content. Note that the noise level is equivalent to about 1.5 cts/min/detector at Yuma and 2.4 at Socorro.

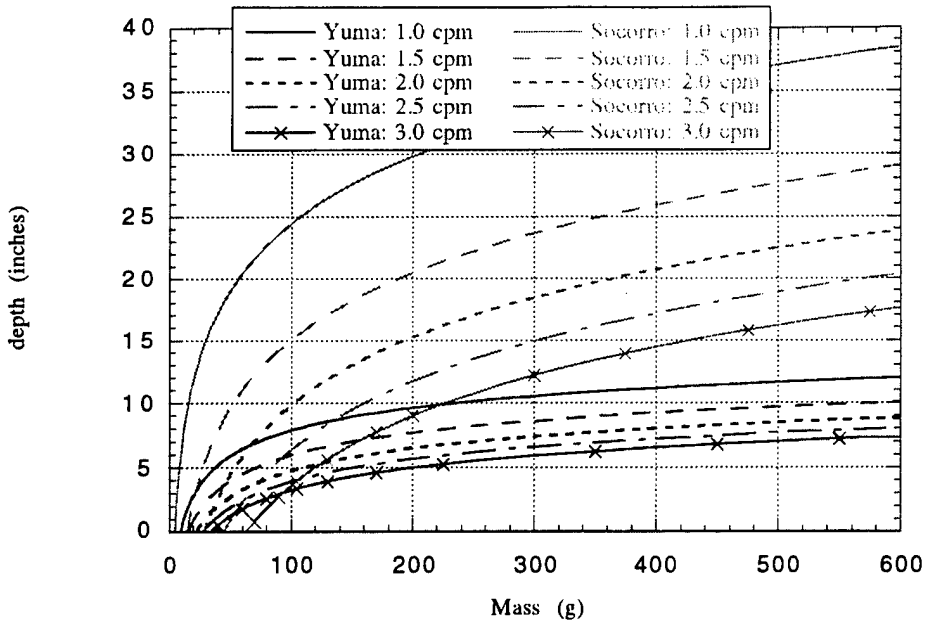

Figure ES-2. Performance at Yuma and Socorro Based on Semi-Empirical Model

It should be noted that the behavior with depth is very different at the two sites. Variability in neutron absorption based on difference in geology is to be expected, but this is a striking example. As discussed in Chapter II, there will be regions where this technique is completely impractical because of rapid neutron absorption in the soil.

In addition, brute force helps. By this we mean that despite the greater difficulty with deep items, the performance at Yuma was better than at Socorro as a result of increasing detector number and counting times. Unfortunately, further increasing the number of detector minutes is not expected to decrease the systematic error. Zeroing the statistical error would only increase the signal to noise by about 40 percent. This is not nearly enough to make the performance operationally interesting. Hardware upgrades to the source or detectors will be necessary for adequate performance.

2. Hardware Upgrades

Hardware upgrades are needed to improve the signal-to-noise ratio from about 1 to about 10 in order to allow for 99-percent P_d with a 10-percent P_{FA}. Simply increasing source strength or counting times will not help much because the systematic error driven by the backgrounds will not be reduced. However, by replacing the continuous isotopic source with a pulsed neutron generator, the energetic neutrons and the thermal neutrons are separated in time. Time gating could be used to eliminate the contribution of the fast

neutrons to the background in the nitrogen region (around 10.8 MeV). More important, the lower energy spectrum would be cleaner, possibly allowing for a more effective background subtraction in the nitrogen region. It is not clear how much improvement is possible by using a pulsed-neutron generator.

The other approach to upgrading the hardware would be to use high-purity germanium (HPGe) detectors, which possess a much finer energy resolution. Right away, this would eliminate the silicon background from the nitrogen region, because the 10.6- and 10.8-MeV peaks would be resolved. The systematic error would be essentially eliminated. In addition, the statistical error from the counting statistics would be greatly improved, because the dominant background source (the Si) would be eliminated, and the contributions from other sources would decrease proportionally to the improvement in energy resolution.

Either of these approaches leads to a more expensive and more complex system to be used in the field. Neutron generators are essentially particle accelerators. The currently available ones require significant moderation of the neutrons. Ge detectors require cryogenic cooling and special handling to avoid "microphonics," or vibration-induced noise in the detectors. If the improvements in performance of either of these approaches are quantified, and adequate, there still will remain operational questions about the utility of the system in UXO clearance.

3. Other Issues Related to Utility of a TNA Explosive Confirmation System

If we assume that either as a result of improved detectors or improved sources, or both, an adequate system performance is obtained, there are still a number of issues to address before it is established that a fieldable system is feasible and useful. These include acquisition and operating and maintenance costs, achievable survey rates, and geographic applicability.

A system using neutron generators with NaI detectors could probably be procured in a ruggedized form for under $1 M each. Operation and maintenance costs would be significant. The system would be heavy and complex. We suspect interrogation times for high P_d low P_{FA} application would continue in the 10-minute range. As indicated above, it is not clear that improved sources alone would give adequate performance. If Ge detectors are required, the cost for a single system would probably be in the $2–3M range. Operation and maintenance costs would again be significant. The system would still be quite complex

because of cooling requirements and the need to prevent microphonic noise in field operation. Interrogation times on the order of 10 minutes would still be required.

The continued long interrogation times means that survey rates would be slow. The overall financial viability for such a system for commercial clean-up involves the cost trade between digging empty holes and operating the TNA system. We do not believe enough information is available at present to make such a cost trade.

Finally, this system will not be employable everywhere. There will be places where the geology does not permit neutron activation because of elevated amounts of neutron scavenging boron or rare earths. In addition, there will be places where the terrain is too rugged for operation of a system of this size and complexity.

Once the technical issues of achievable performance are settled, these issues can be faced.

D. CONCLUSION AND RECOMMENDATION

Thermal neutron activation to detect energetic materials via their nitrogen content is a promising approach to improving unexploded ordnance remediation. This approach cannot be used in rapid search, but could be used to confirm the presence of hazardous materials, after another sensor has identified a location of potential interest. The demonstration of the NVESD/SAIC system at Socorro and Yuma serves as a proof of concept. The performance corresponds to an effective signal-to-noise ratio of about one, which is too poor for operational utility. Increasing the effective signal to noise of a fieldable system to about 10 would be required for adequate technical performance.

Two approaches to upgrading the hardware have been identified, aimed at improved sources and improved detectors, respectively. Getting adequate improvement from new sources will require a significant reduction in the systematic errors associated with the background subtraction algorithm. This possibility cannot be ruled out, but is very challenging. A more likely, and more expensive, approach is via improved detectors with much better energy resolution. In this case, we believe the background can be reduced, leading to both reduced statistical errors, and essential elimination of the systematic errors associated with the background subtraction.

Improved technical performance is not a guarantee of operational utility in this case. Once the performance is determined, it is necessary to look at the operation costs of such a system compared to the savings from reducing the number of false alarms investigated.

Significant improvements in the ability to discriminate ordnance from nonordnance items using other sensors would make the economic feasibility of using this system less likely.

In spite of all these difficulties, we regard TNA as a promising technology which warrants continued investigation to determine the performance limits of a fieldable system.

I. INTRODUCTION

Unexploded ordnance (UXO) is a significant problem on many current and former U.S. military bases. As much as 11 million acres in the United States may be contaminated. This UXO poses a hazard to active-duty personnel on test and training ranges. UXO is also a hazard to the general population on formerly used defense sites (FUDS) that have already been released, and it is an impediment to the further transfer of land on closing bases. Current methods of UXO clearance are laborious, time consuming, and often ineffective. Probabilities of detection are estimated to be in the 80-percent range. False alarms are much more numerous than actual UXO detections, with many more holes dug than buried ordnance recovered. The Services routinely cite better methods for UXO clearance as high priority cleanup needs.

For these reasons the Environmental Security Technology Certification Program (ESTCP) has invested in the development and demonstration of a number of technologies aimed at improving remediation of ordnance-contaminated sites. In one of these projects, ESTCP provided funds to the Night Vision and Electronic Sensors Directorate (NVESD) for the Remote Controlled Surface/Near Surface UXO detection system. This system includes a remote-controlled vehicle, a Scheibel electromagnetic induction sensor for rapid search of large areas, and a thermal neutron activation (TNA) sensor for confirmation of energetic material associated with the metal detected by the induction sensor.

This paper focuses on the performance of the TNA sensor in its confirmation role. TNA itself is too slow for large area searches. Its advantage over traditional UXO sensors is that it responds to concentrations of nitrogen, which, although very rare naturally, are characteristic signatures of energetic materials. Most UXO systems use a detection scheme which responds to the metal casings associated with ordnance. The TNA sensor attempts to detect the presence of the explosive itself, which leads to the possibility of greatly reduced false-alarm rates.

The TNA sensor system developed in this program was based on earlier work at Science Applications International Corporation (SAIC) for explosive detection in airport luggage searches and in countermine applications. The TNA system was tested at Socorro, New Mexico, and Yuma, Arizona. The results of these tests are sufficient to allow some

quantitative statements about performance and also some predictions about the performance to be expected as a result of some possible hardware upgrades.

Chapter II explains the phenomenology of TNA as a detection scheme for nitrogen concentrations in soil. Chapter III is an analysis of the data from Socorro and Yuma. Chapter IV discusses hardware issues and the prospects for improved performance.

II. THERMAL NEUTRON ACTIVATION: THEORY AND PHENOMENOLOGY

A. INTRODUCTION

TNA is a technique for identifying the presence of particular nuclear isotopes in a sample of material. The sample is bathed with thermal neutrons, which are captured at various rates by the atomic nuclei present. In most cases, this capture process results in a gamma (γ) ray. The spectrum of γ rays that emerges is unique for each species of atomic nucleus. In principle, one can determine the composition of material by irradiating it with neutrons and measuring the resulting spectra.

In some applications, such as oil exploration, this technique has proven quite successful for geological characterization. Above ground, TNA has been applied to the detection of explosives in airplane luggage and other containers. The technique has been proposed for mine detection and the detection of surface and near-surface UXO by building on the approach used in luggage examination. This technique will be challenging to apply to underground explosive detection because the amounts of explosive are small compared with deposits of geological interest, yet unlike the case of above-ground detection, there will be complicated backgrounds from the irradiation of the soil.

The approach is limited by both hardware and background issues. First, the detection systems have finite resolution and relatively low efficiency. The finite resolution means that the characteristic peaks from different atomic nuclei will overlap. Any attempt to detect small quantities of a material in the presence of many other nuclei with the current detectors will lead to an essentially smooth overall spectrum with few distinguishing features readily tied to any of the component nuclei. This problem is directly related to the background issue—to identify and estimate the small quantities that may be present, the backgrounds from the more common materials must be determined and subtracted. The low overall efficiency of the process makes the background subtraction and target identification more difficult because of statistical fluctuations in the number of counts observed.

The next sections will discuss these issues in more detail, focusing first on the thermal neutron transport, capture, and ensuing photo-emission, and then on data analysis and hardware issues.

B. THEORY AND PHENOMENOLOGY OF THERMAL NEUTRON ACTIVATION

1. Interaction of Neutrons With Matter

Neutrons are neutral particles that together with protons make up the atomic nucleus. Because they are electrically neutral, their interaction with matter requires proximity to the atomic nuclei leading to relatively long paths in matter compared with charged particles. At energies characteristic of neutrons produced by fissioning nuclei (around 1 MeV or below), the dominant (and often the only energetically allowed) reactions are elastic scattering and neutron capture. A fission neutron traveling in matter will typically undergo many elastic scatterings, transferring energy to the scattering nuclei until it is "thermalized," or slowed to the point where it is equally likely to acquire energy from the collision as to lose it. The process of slowing neutrons by elastic scattering is called moderation. The resulting "thermal" neutrons continue to propagate and scatter until they are captured by a nucleus, forming a highly excited state of a new nucleus with one higher mass number. In most cases, this state decays by emitting a γ ray, although for some nuclei a proton or an alpha particle can be emitted.

a. Elastic Scattering and Thermalization

At energies below 1 MeV or so, the elastic scattering cross section is approximately constant, and is typically a few barns (1 b = 10^{-24}cm^2). The resulting mean free path in typical soil is a few centimeters. The scatterings transfer energy to the recoiling nucleus. The lighter the target nucleus, the more forward peaked the process and the higher the energy loss on average. (This is true even though for a given nucleus, the more forward peaked a particular scattering, the lower the energy loss.) For example, for hydrogen, a neutron loses on average half its energy per collision, with half the scattering forward of 45 degrees. For oxygen, a neutron loses on average 11 percent of its energy, with half the scattering forward of 86.4 degrees. Scattering from oxygen and heavier elements is essentially isotropic and turns the propagation into a random walk. This means that the total path length for a propagating neutron can be much longer than the total distance traveled. (See Figure II-1.)

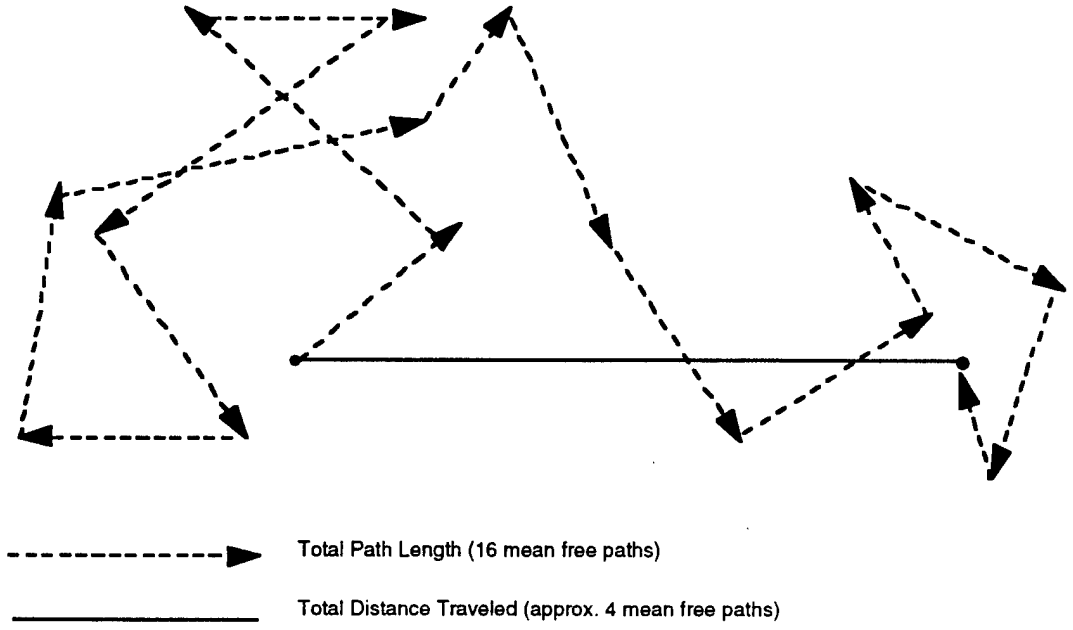

Figure II-1. Neutron Scattering: Path Length vs. Net Distance Traveled

Of primary relevance to this application of TNA is how far an energetic neutron travels before thermalization. This distance depends critically on the presence of low atomic mass materials in the soil, because the neutrons transfer more energy to lighter collision partners. The nominal energy of a thermal neutron is 0.0253 eV. Therefore, thermalization of a 1-MeV neutron would require about 150 collisions with oxygen. The total distance traveled would be approximately $\sqrt{150}$, or only 12–13 mean free paths. This illustrates a second important consequence of the elastic scattering—the neutrons are "localized" by the random walk nature of the transport. This localization continues to be a feature of the elastic scattering even after the neutrons have thermalized.

The presence of water is important because it is the dominant source of hydrogen in the soil. In collisions with protons (i.e., hydrogen nuclei), the neutron loses on average half its energy, and can lose it all in a single "head-on" collision. On average, 25 collisions would suffice for thermalization of a 1-MeV neutron.

Two implications follow for the use of fission neutrons for TNA systems of the half-meter diameter size under consideration. First, the typical mean free paths for thermalization are sufficiently long that a moderator will be needed if there is not to be a reduced density of thermal neutrons near the source. Second, the TNA system is physically large enough that the random walk nature of the transport manifests itself within

the area being interrogated. Within this area, the thermal neutron flux is attenuated over physical distances in the ground much shorter than the mean free path for attenuation.

b. Capture Processes

There are two major differences between neutron capture and elastic scattering. First, the capture cross section is inversely proportional to the velocity, so it increases as the energy decreases. Second, the capture cross sections vary enormously from nucleus to nucleus.

Thermal neutron capture is an exothermic reaction. Hence, it proceeds at a fixed rate if the neutron is near the nucleus. The 1/v dependence therefore can be understood as deriving from the time the neutron spends in the vicinity of the nucleus. Because the capture processes are so much more likely for thermal neutrons, energetic neutrons must be reduced to thermal energies or "moderated" by elastic scatterings before neutron capture becomes probable.

The variation of cross section with target nucleus can also be understood qualitatively. There are two steps to the process: formation of a compound nuclear state and decay of that state to a bound state of the final nucleus. Both these steps will have rates which vary greatly from nucleus to nucleus.

First, the neutron and the target nucleus of mass A form a compound nuclear state in the nucleus of mass A+1. The states of allowed spin and parity in the compound nucleus will in general not perfectly match the energy of the thermal neutron plus the target nucleus system. The better the match, the higher the yield, according to the Breit-Wigner relationship for resonant processes.

This compound state then decays by emitting a photon to a lower state within the A+1 nucleus. This emission requires a strong electromagnetic matrix element between the states. In other words, the nuclear states need to have similar structure. For a few nuclei, emission of alpha particles or protons is energetically allowed. The strong interaction matrix elements associated with these reactions gives them large cross sections. For the bulk of nuclei that delay electromagnetically, electric dipole or magnetic dipole transitions will usually be the strongest, because even for energetic decays, the product of the wavenumber and the nuclear radius is small. Finally, the phase space factor, which is proportional to the square of the photon energy, is important.

Because of the importance of dipole transitions, heavy nuclei filling p-shells have large capture cross sections. This includes iron region and rare earth elements. Nitrogen has a proton-emission mode, and as a result less than 5 percent of the neutrons captured on N yield a photon. Boron captures neutrons via the (n,alpha) reaction. The presence of boron or rare earth elements in the soil greatly increases neutron attenuation. On the other hand, the most common element in soil, oxygen, has a very low neutron-capture cross section. The capture mechanisms are discussed in somewhat more detail for nitrogen and oxygen in Appendix A.

2. The Nature of Soil and Explosives as it Pertains to Neutron Propagation

Table II-1 gives the composition in percentage by weight and by atomic number density of the most common elements in the Earth's crust, along with the thermal neutron absorption and scattering cross sections.[1] The number densities are computed assuming a density of 2 g/cm^3 for the soil. The cross-section columns are followed by columns giving the "Macroscopic Cross Section" (symbol: Σ) or the product of the cross section and the number density. The mean free paths for interaction are equal to the reciprocal of the sum of the individual Σ's, and appear at the bottom of the column. Table II-2 gives values for boron and gadolinium, which are important for this application but rare in most "typical" soil, and for water, which is highly variable. The values shown in Table II-1 are representative of sites like Socorro and Yuma, but in many other areas the naturally occurring nitrogen will add to the background.

The largest component of the Earth's crust is oxygen. In dry earth it is the dominant element during the thermalization process because of a combination of its abundance and high neutron scattering cross section. The large cross section serves both to thermalize the neutrons and to effectively "localize" (defined below) them. We see from Table II-1 that the oxygen alone in the crust would result in approximately a 7-cm mean free path for thermalized neutrons (the reciprocal of the macroscopic cross section). At 1 MeV, the scattering cross section is 8 b, and the mean free path is only 3.6 cm. The scattering is as likely to produce a backward traveling as forward traveling neutron, so the neutron propagation is essentially a random walk. Because the distance traveled in a random walk

---

[1] Not taken into consideration is the considerable organic material—and thus substantially elevated nitrogen levels—found in most surface earth.

Table II-1. Neutron Transport Properties of Common Soil Elements

	Percent by Weight	Number Density	Thermal Neutron Absorption Cross Section (b)	Absorption Factor or Macroscopic Cross Section Σ (cm^{-1})*	Thermal Neutron Scattering Cross Section (b)	Scattering Factor or Macroscopic Cross Section Σ (cm^{-1})*
0	46.1	3.47E+22	0.00027	9.37E–06	3.76	0.131
Si^{28} (and Si^{30})	27.6	1.19E+22	0.16	1.90E–03	2.2	0.026
Si^{29}	1.6	6.65E+20	0.12	7.98E–05	2.2	0.001
Al	8.2	3.66E+21	0.23	8.42E–04	1.49	0.005
Fe	5.6	1.21E+21	2.55	3.08E–03	10.9	0.013
Ca	4.2	1.26E+21	0.43	5.43E–04	3.03	0.004
Na	2.4	1.26E+21	0.53	6.66E–04	3.2	0.004
K	2.1	6.47E+20	2.1	1.36E–03	1.5	0.001
Ti	0.6	1.51E+20	6.1	9.21E–04	4	0.001
H	0.1	1.20E+21	0.332	3.97E–04	21	0.025
Total	98.5	5.66E+22		9.80E–03		0.207
			MFP (cm) =	102	MFP (cm) =	4.82

* The attenuation rate is given by the product of the cross section and number density. The sum of the attenuation rate is the reciprocal of the mean free path (MFP).

Table II-2. Neutron Transport Properties of Rare Soil Elements

	Percent by Weight	Number Density	Thermal Neutron Absorption Cross Section (b)	Absorption Factor or Macroscopic Cross Section Σ (cm^{-1})*	Thermal Neutron Scattering Cross Section (b)	Scattering Factor or Macroscopic Cross Section Σ (cm^{-1})*
Common Soil Elements	98.5	5.66E+22		9.80E–03		0.207
H_2O	5	3.16E+21	0.662	2.09E–03	103	0.325
B	0.001	1.05E+18	759	7.99E–04		
Gd	0.0006	4.34E+16	49000	2.13E–03		
Total		5.98E+22		1.48 E–02	103	0.533
			MFP (cm) =	67.5	MFP (cm) =	1.88

* The attenuation rate is given by the product of the cross section and number density. The sum of the attenuation rates is the reciprocal of the mean free path.

increases as the square root of the number of steps, for a 1-MeV neutron to get to a location 36 cm from its starting point it would undergo on average 100 (not 10) collisions. Thus, while the total path length would be 360 cm, the net distance traveled in one direction is only 36 cm. In addition, the direction of net travel will be uncorrelated with the initial neutron direction. This is what we mean by localized.

Table II-2 shows that modest soil moisture (5 percent) dramatically reduces the mean free path because of the large cross section for water. This reduction is in part because at thermal energies, the atomic cross sections do not sum to give the total molecular cross section. The measured cross section for water, 103 b, is much higher than that obtained by summing the oxygen and twice the hydrogen cross sections. At higher energies, the cross sections do sum, and the contributions from water become relatively smaller, although they are still significant. At 1 MeV, for example, the hydrogen cross section is 3 b and the oxygen cross section is 8 b, giving 14 b for H_2O.

The phenomenology can be summarized as follows. There are very short mean free paths for neutrons in soil, just due to the presence of oxygen. Oxygen is ubiquitous in soil, being the most common element in almost all minerals. There is some variability with energy and soil moisture. In general, mean free paths will be on the order of a few centimeters, and thermalization distances on the order of a few 10s of centimeters at most. In general, except for very moist soils, fission neutrons will have to be moderated to some extent before entering the soil.

The neutron absorption process is much slower than the scattering. Table II-1 shows that for each of the common elements the cross section for absorption is less than the scattering cross section. The common elements in dry soil together would produce a mean free path of just over 100 cm for thermal neutrons. However, once thermalized, the neutrons are captured locally. This is because the "random walk" propagation due to the elastic scattering localizes the neutrons as discussed above. A neutron source and moderator can therefore be designed which will produce neutron captures more or less uniformly over a reasonably sized region.

In Table II-1, silicon has a separate entry for the mass 29 isotope. About 1 percent of the total number of captures in typical soil will occur on Si^{29}, and 7.6 percent of those will yield a 10.6-MeV γ ray, which is the primary background from which the nitrogen counts must be extracted. For 1 million neutrons captured in "typical" soil, we expect 620 10.6-MeV γ rays from the Si^{29} background. In contrast, a 0.1-percent admixture of nitrogen to typical soil would capture about 1.6 percent of the neutrons, but only .57 per-

cent of those would yield a 10.8-MeV γ to the ground state. For 1 million neutrons captured by typical soil with a 0.1-percent admixture of nitrogen, about ninety-five 10.8-MeV γ rays would result.

Table II-2 shows that the neutron-absorption process will be much more variable than the scattering. The average amounts of boron and gadolinium in soil (.001 percent and 6×10^{-4} percent, respectively) would increase the absorption rate by one-third. Soil with 5-percent moisture would show more than a 20-percent increase in the absorption rate over dry soil. Increased amounts of boron or rare earth elements, including gadolinium, would dramatically reduce the path length for absorption and would reduce the depth at which the technique could work.

For example, Table II-2 shows that the average admixture of boron and gadolinium, with 5 percent water to the common elements in dry soil leads to a mean free path for absorption two-thirds the value of dry soil alone. If elevated amounts of boron or rare earth elements are considered the effects are even more dramatic. A boron concentration of .01 percent with 5 percent water would cut the mean free path in half. A gadolinium concentration of .01 percent would dominate the absorption and cut the mean free path by a factor of three.

We have not looked at the geological issues in any detail; however, there will clearly be regions where concentrations of rare elements with very large absorption cross sections render this technique impractical.

Even for relatively benign soils with no boron or rare earth elements, detection of items buried more than about 30 cm will be limited by the neutron absorption along the path. This limitation is in large part because the scattering cross section makes the propagation random-walk like, so the resulting path length is many times the physical depth.

We turn now to neutron propagation through a typical explosive—in this case, RDX ($C_3H_6N_6O_6$), with percentages and cross sections given in Table II-3. We noted above in the case of water that for thermal neutrons, molecular cross sections are not given by the sum of the constituent atomic cross sections. Nevertheless, since we are not aware of any measurements of the cross section of thermal neutrons and RDX, we assume the cross sections simply add. This is likely to be an underestimate. We see that largely because of the scattering from hydrogen, the mean free path is about 1 cm, significantly

Table II-3. Neutron Transport Properties of RDX

RDX	Percent by Weight	Number Density	Thermal Neutron Absorption Cross Section (b)	Attenuation Rate or Macroscopic Cross Section Σ (cm^{-1})*	Thermal Neutron Scattering Cross Section (b)	Scattering Rate or Macroscopic Cross Section Σ (cm^{-1})*
H	3	2.93E+22	0.332	9.73E–03	21	0.62
C	16	1.47E+22	0.0034	4.98E–05	4.75	0.07
N	38	2.93E+22	1.85	5.42E–02	10.6	0.31
O	43	2.93E+22	0.00027	7.91E–06	3.76	0.11
Total Σ				0.064		1.11
Mean free path				15.63 cm		0.9 cm

* The attenuation rate is given by the product of the cross section and number density. The sum of the attenuation rate is the reciprocal of the mean free path.

shorter than for typical soils. Traversing a large ordnance item, say, a 10-cm path through explosive in a 105-mm shell, would involve on average about 100 elastic scatterings, for a total path length of 100 cm.

The short mean free path has two effects. First, since the neutrons are better localized by the short mean free path, there will be an enhancement of the neutron capture within the explosive material relative to the soil, which will increase the signal. Second, the large capture rate to undesired channels, dominated by the N(n,p) reaction, will prevent the neutrons from fully sampling the nitrogen in large ordnance items. The second effect works to limit the first, at least for large ordnance items. Traversing 10 cm of RDX, or 10 mean free paths, would typically involve 100 scattering events during a 100-cm random walk. This is about six mean free paths for absorption. Thus, using the numbers from Table II-3, the flux across 8 cm of explosive would be reduced by a factor of about 100 by the capture process. This will significantly decrease the counts in the desired channels for medium or large ordnance items. The combination of the short mean free path for scattering and the large N(n,p) absorption leads to the nitrogen screening itself when present in the amounts characteristic of medium to large ordnance items. For TNT, which is especially low in nitrogen and hydrogen, more modest effects are expected. However, even in this case, the scattering and absorption mean free paths are both shorter than expected for the Earth's crust, and hence, self-screening of the nitrogen is predicted for TNT as well. This attenuation through large ordnance items is observable in the data from Socorro and Yuma and is modeled in Chapter III.

C. SUMMARY

The idea behind using TNA to detect explosives is to use the high-energy γ ray (10.8 MeV) resulting from the capture on N^{14} as a signature for the presence of concentrations of nitrogen. This is one of the highest energy γ rays resulting from neutron capture, so backgrounds are small. Concentrations of nitrogen occur in all explosives, but only rarely in nature. This combination of facts makes using TNA an attractive means to attempt to identify unexploded ordnance.

The first step in applying TNA to the detection of unexploded ordnance is injection of neutrons of varying energies into the soil. These neutrons are moderated and localized by the large amounts of oxygen in the soil. The moderation results from the loss of energy when scattering from the light atomic nuclei in the soil, and the localization results from the scattering turning the propagation into a random walk wherein the path length is large

compared to the net distance traveled. There will be some variability with energy spectrum, the detailed composition of the soil, and moisture content; however, the moderation and localization are universal phenomena.

After moderation of the neutrons, capture by atomic nuclei becomes increasingly likely. For this process the oxygen in the soil is largely irrelevant because of its low capture cross section. The important elements common in soil are silicon and iron, accounting for about half the absorption due to the common elements. Silicon is also important because capture on the mass 29 isotope leads 7.6 percent of the time to a 10.6-MeV gamma ray, which is the primary background for the N^{14} detection scheme based on the 10.8-MeV gamma. This means that any TNA approach will need either good resolution or a robust background subtraction scheme to estimate the Si contribution. If there is a lot of organic matter in the soil with its attendant nitrogen, one might need a background subtraction scheme even with high resolution.

A number of rare elements are important also. Boron and most of the rare earth elements, especially gadolinium, have very high neutron capture cross sections. As a result, any significant concentration of these elements to a few times their average density will interfere significantly with the applicability of TNA to nitrogen detection. Even in the most benign soils, attenuation is likely to limit detection to the top 30 cm or so.

The large nitrogen capture cross section for the N(n,p) process leads to self-screening by large amounts of explosive. The attenuation of neutrons due to the nitrogen keeps the signal from increasing linearly with the mass of nitrogen. One of the implications of the self screening is that deeply buried large items cannot be detected—you cannot make up for the attenuation with depth very effectively by increasing the amount of nitrogen in the sample.

For the system at hand, there is an inherently low signal to background, resulting primarily from the silicon in the soil. After background subtraction, there remains a challenging signal-to-noise (S/N) level, where the noise is partly due to counting statistics and partly due to the modeling of the subtracted background. These features trace directly to the scattering and attenuation issues discussed above. Details of the tests at Yuma and Socorro and possible hardware responses to these challenges are discussed below.

III. PERFORMANCE AT ESTCP TESTS

In this chapter, we derive a semi-empirical formula for the expected signal as a function of the target's mass and location. The functional form we use is greatly simplified. It is developed from theoretical considerations (with knowledge of the data) in Section A, and the free parameters are determined by fits to data taken at Yuma, Arizona, and Socorro, New Mexico, in Section B. In Section C, we compare the performance of the system at Yuma to that at Socorro.

A. THEORETICAL PREDICTION OF SIGNAL

We begin by considering the expected dependence of the signal strength on the target's mass. The number of counts contributing to the signal due to neutrons traveling a distance between x and x + dx in the target will equal the number of neutrons that have survived up to the distance x times the number that undergo an N^{14}(n,γ-to-ground) reaction in the distance dx. In equation form:

$$\frac{\#\text{counts}}{\text{sec}} = I(x)AN\sigma_{(n,\gamma)}dx \quad , \tag{3.1}$$

where I(x) is the neutron beam intensity at x in number of neutrons per area-second; A is the cross sectional area, which we assume does not vary much with x; N is the number of nitrogen atoms per cm^3; and $\sigma_{(n,\gamma)}$ is the N^{14}(n,γ-to-ground) cross section (= 0.011 b). I(x) is given by

$$I(x) = I_0 e^{-\Sigma_{tot-abs}x} \quad , \tag{3.2}$$

where I_0 is the neutron intensity when the beam first hits the target, and $\Sigma_{tot\text{-}abs}$ is the total macroscopic cross section for neutron absorption, given by

$$\Sigma_{tot-abs} = \sum_i N_i \sigma_{i-abs} \quad , \tag{3.3}$$

where N_i is the number density of the ith isotope, $\sigma_{i\text{-}abs}$ is the total cross-section for all neutron-absorbing reactions of the ith isotope, and the sum is over all isotopes in the target. The only neutron-absorbing reactions with significant cross sections in an explosive are N^{14}(n,p) with σ = 1.77 b, H(n, γ) with σ = 0.33 b, and N^{14}(n,γ) with σ = 0.075 b.

After plugging Eq. (3.2) into Eq. (3.1) and integrating over the total path length traveled, L, we obtain

$$\frac{\text{total\#counts}}{\text{sec}} = \frac{I_0 A N \sigma_{(n,\gamma)}}{\Sigma_{\text{tot-abs}}}\left[1 - e^{-\Sigma_{\text{tot-abs}} L}\right] \quad . \tag{3.4}$$

If the linear dimension, X, of the target is greater than a few mean free paths (as it will be for most targets of interest), the total path length will not equal the linear dimension, because the neutrons do not travel in a straight path; rather, they undergo large-angle elastic collisions with the nuclei constituting the target. The path length is

$$L = n \cdot \text{mfp} \quad , \tag{3.5}$$

where n is the total number of elastic collisions, and mfp is the mean free path. The distance traveled in one dimension is

$$X = \sqrt{n} \cdot \text{mfp} \quad , \tag{3.6}$$

and the mean free path is

$$\text{mfp} = \left(\Sigma_{\text{tot-elastic}}\right)^{-1} \quad , \tag{3.7}$$

where

$$\Sigma_{\text{tot-elastic}} = \sum_i N_i \sigma_{\text{i-elastic}} \quad , \tag{3.8}$$

and $\sigma_{\text{i-elastic}}$ is the cross section for an elastic collision with a thermal neutron for the ith isotope in the target. Thus,

$$L = \frac{X^2}{\text{mfp}} = X^2 \Sigma_{\text{tot-elastic}} \quad . \tag{3.9}$$

If we approximate the volume as X^3 and the area A as X^2, then $A \sim (M_{exp}/\rho_{exp})^{2/3}$, and $L \sim \Sigma_{\text{tot-elastic}}(M_{exp}/\rho_{exp})^{2/3}$, where M_{exp} is the mass of the explosive, and ρ_{exp} is its density. Further, if we assume that the mass of nitrogen is proportional to the mass of explosive, then the expected dependence of the signal strength on the nitrogen mass, M, is

$$\frac{\text{total\#counts}}{\text{sec}} \propto M^{2/3}\left[1 - e^{-\beta M^{2/3}}\right] \quad . \tag{3.10}$$

We can estimate the value of β as follows. From above,

$$\beta = \frac{3^{2/3}\sum_i N_i\sigma_{i\text{-abs}}\sum_i N_i\sigma_{i\text{-elastic}}}{\rho_{exp}^{2/3}}$$

$$= \frac{3^{2/3}[X(0.33\,b)+Y(1.85\,b)][V(4.75\,b)+X(20.5\,b)+Y(10.0\,b)+Z(3.78\,b)]}{\rho_{exp}^{2/3}}\left(\frac{N_A\rho_{exp}}{A_{exp}}\right)^2$$

(3.11)

where $C_VH_XN_YO_Z$ is the chemical formula for the explosive, N_A is Avogadro's number, A_{exp} is the gram atomic weight of the explosive, and the nitrogen mass is assumed to be one-third the total mass of the explosive. (This percentage will vary from about 28 to 34 percent for the explosives used at the Yuma and Socorro test sites.) We have also assumed that the nuclei constituting the explosive molecule act independently of one another when they interact with neutrons. This is true for neutron absorption but not necessarily for neutron elastic scattering, particularly at thermal energies. To be more precise, experimental measurements of the cross sections of thermal neutron elastic scattering off the explosive molecules must be used. For order-of-magnitude estimates, however, this approximation should suffice.

If the density and gram atomic weight of all explosives are similar, and we use RDX ($N_6C_3O_6H_6$) as our representative explosive, then ρ_{exp} = 1.8 g/cm^3, A_{exp} = 222, and β = 0.096 g$^{-2/3}$. However, this is an overestimate because the elastic collisions with hydrogen will not scatter the neutrons as much as those with carbon, nitrogen, and oxygen. If we calculate β without the elastic collisions with hydrogen, then β = 0.042 g$^{-2/3}$. Thus, we estimate that β lies between 0.04 and 0.1 g$^{-2/3}$. We will find that this is in good agreement with the Yuma data.

Note that Eq. (3.10) implies that the signal strength will not increase linearly with mass (or equivalently, volume), but rather, for a large mass, the signal will increase only as $M^{2/3}$ (or projected area). Physically, this is because, as the neutron beam travels through the target, the neutrons are "eaten up" by the $N^{14}(n,\gamma)$, $N^{14}(n,p)$, and $H(n,\gamma)$ reactions. From a practical standpoint, we might not expect to see this "saturation effect" if we considered only the $N^{14}(n,\gamma)$ reaction, because the cross section for this reaction is fairly small, and in this case, the coefficient β would be very small. Further, if we neglected the effect of the elastic collisions, then the path length would be proportional to X rather than X^2. In this limit [including only the $N^{14}(n,\gamma)$ reaction and ignoring elastic scattering], we estimate $\beta \approx 0.0026$ g$^{-1/3}$, using RDX as our representative explosive. In this case, the argument of the exponent is small even for the 105-mm shells, and we would obtain:

$$\frac{\text{total\#counts}}{\text{sec}} \propto M^{2/3}\left[1-(1-\beta M^{1/3})\right] \propto \beta M \quad . \tag{3.12}$$

Note, however, that if we include both the $N^{14}(n,p)$ and $H(n,\gamma)$ reactions, while still ignoring scattering, $\beta \approx 0.076\ g^{-1/3}$, and thus Eq. (3.12) would apply only for small masses (20 or 30 mm). We will show in the data analysis section below that Eq. (3.10), rather than (3.12), is the model that better describes the data.

Next, consider the dependence of the signal strength on the target position. In general, the signal should decrease as either the neutrons or the γ-rays travel through the soil. (There are additional complicating factors, such as moderation of fast neutrons adding to the flux and geometric factors having to do with source and detector finite size.) To keep our parameterization as simple as possible, we represent the dependence of the signal on the depth of the ordnance as:

$$\frac{\text{total\#counts}}{\text{sec}} \propto e^{-\alpha\cdot\text{depth}} \quad . \tag{3.13a}$$

The choice of an exponential fall-off follows because, overall, both the neutron and γ-ray intensities will decrease exponentially with distance traveled. The parameter α will be a function of the soil composition and of the cross sections for both neutron and γ-ray interactions with the atoms in the soil. We emphasize, however, that Eq. (3.13a) represents a simple model. Equation (3.13b) is a slightly more complicated function which explicitly incorporates the fact that the number of γ-rays reaching the detector will be proportional to the solid angle subtended by the detector. Ignoring offset, this proportion will be given by the detector area divided by the square of the depth:

$$\frac{\text{total\#counts}}{\text{sec}} \propto \frac{e^{-\alpha\cdot\text{depth}}}{(\text{depth}+h)^2} \quad , \tag{3.13b}$$

where h is the height of the detector. But even Eq. (3.13b) is relatively simple, because it neglects the fact that the majority of neutrons are not thermalized before they penetrate the soil. (The average neutron energy leaving the SAIC system is about 1 MeV.) While the total neutron flux will decrease exponentially from the surface, the thermal neutron flux may increase over the first inch or so, as the neutrons undergo elastic collisions (moderation) with atoms in the soil. Thus, the dependence of the thermal neutron flux on distance over the first few inches of soil will depend on the composition and moisture content of the soil as well as on the neutron energy spectra at the soil surface.

We fit the Yuma data using both Eqs. (3.13a) and (3.13b) and found no difference in the quality of the fit. Furthermore, for the Yuma data, both Eqs. (3.13a) and (3.13b)

yield identical predictions of the Si background counts. (We perform this calculation in the data analysis section below as a test of the quality of our fits.) On the other hand, the Socorro data is not easily fit to the functional form given in Eq. (3.13b); the minimization procedure we use yields a value of α which is negative (i.e., a positive coefficient in the exponent). We have thus chosen to utilize Eq. (3.13a).

Thus, our theoretical prediction for the signal as a function of nitrogen mass and target depth is the following:

$$\text{Signal} = C + BM^{2/3}\left[1 - e^{-\beta M^{2/3}}\right]e^{-\alpha * \text{depth}} \quad . \tag{3.14}$$

B, α, and β will be determined from a fit of the measured data described in Section B below. C represents the residual background signal after subtraction of the estimated background in the absence of explosives, and is also determined from measurements.

Detectors are arranged in a ring, so to be complete, we should also include a term to account for horizontal offset. However, this effect is even more difficult to model than the depth dependence. Although signal strength can be reasonably expected to decrease with depth, no such simple claims can be made about offset. For example, consider the following two competing effects. Because the detectors are arranged in a ring, if one had a constant γ-ray source that one were trying to detect, the signal averaged over all detectors would increase as the γ-ray source moved from the center of the ring to one of the edges. This increase occurs because the number of γ-rays reaching a detector is proportional to the solid angle subtended by the detector, which varies inversely with the square of the distance. (This effect would be magnified by the γ-ray attenuation in the soil. However, the mean free path of a 10 MeV γ-ray in typical soil is about 8 to 10 inches, so γ-ray attenuation is not a strong factor.) However, the γ-ray source is *not* constant; it decreases as it is moved from the center to the edge, because the thermal neutron flux decreases from the center to the edge (neglecting moderation effects). Whether there will be an increase or decrease with offset, then, depends on whether neutron attenuation in the soil is more or less important than geometric effects combined with γ-ray attenuation. We postulate that the two effects are comparable, because the measured signals from both the Yuma and Socorro tests do not seem to depend on offset in any statistically significant way.

B. MEASURED SIGNAL

We have used the data from both the Yuma test and from the Socorro test, excluding data points with documentation that was conflicting or unclear. To obtain the

values for B, α, and β in Eq. (3.14), we used the target data, which consisted of 152 data points from Yuma and 128 data points from Socorro. To obtain C, we used measurements on both soil and on mortars with explosives removed (inerts) from Yuma data, and we used inert measurements from Socorro. (There were 2 inerts and 90 soil measurements at Yuma, and 60 inerts at Socorro.) From the Yuma data, we determined that the average background signal was 0.42 cpm, with a standard deviation of 1.5 cpm. From the Socorro data, the average background signal was 0.59 cpm, with a standard deviation of 2.4 cpm.[2] Thus, C in Eq. (3.14) is 0.42 for the Yuma data and 0.59 for the Socorro data.

We note that the statistical error at Yuma was reported to be 0.95 cpm; thus, the systematic[3] error was about 1.1 cpm. At Socorro, the statistical error was poorer by a factor of $\sqrt{3}$ because eight detectors were used rather than twelve, and the measurement time at Socorro was only 5 minutes rather than 10. Given these facts, the statistical error was about 1.65 cpm, implying that the systematic error was about 1.75 cpm. In both cases then, the systematic errors were as large as the statistical errors. In other words, even if one were to count for infinite time, the errors would still be significant.

To obtain estimates of the values for B, α, and β in Eq. (3.14), we first calculated the average value of the signal at each mass and depth, for both the Yuma data and the Socorro data. We then used MATLAB to find the minimum of the error function, defined as

$$\text{error} \equiv \sum_{i=1}^{N}\left[\left(C + BM_i^{2/3}\left(1 - e^{-\beta\sqrt{M_i}}\right)e^{-\alpha * \text{depth}_i}\right) - S_i\right]^2 \quad , \tag{3.15}$$

where N = the number of data points (27 for the Yuma data and 20 for the Socorro data), M_i is the mass of the *ith* data point, depth_i is the depth of the *ith* data point, and S_i is the measured signal of the *ith* data point. Tables III-1 and III-2 show these values, and Table III-3 shows the results of the minimization.

---

2 These numbers all refer to the values after the background subtraction algorithm was applied.

3 "Systematic" is a term used to describe all errors not associated with counting statistics. However, the "systematic" errors are dominated by errors in the background subtraction algorithm which are "noise-like" and hence can be assumed to add in quadrature with the errors associated with counting statistics.

Table III-1. Yuma Data

Explosive Type	Nitrogen Mass (g)	depth = 0	depth = 1"	depth = 2"	depth = 3"	depth = 6"	depth = 12"
20-mm round	3.53	1.00	0.57	------	------	------	------
30-mm projectile	7.9	1.54	1.00	------	0.74	------	------
100 g C4	34	4.00	1.45	2.62	------	1.36	0.78
40-mm projectile	39.6	2.08	------	2.29	------	1.73	------
200 g C4	68	------	------	1.89	------	1.76	3.15
60-mm mortar	111.1	------	------	3.99	------	2.08	------
81-mm mortar	200	------	------	7.89	------	3.29	1.07
2.5 lb C4	378.3	------	------	11.98	------	4.29	1.60
105-mm projectile	609.3	------	------	14.48	------	2.16	1.16

Table III-2. Socorro Data

Explosive Type	nitrogen mass (g)	depth = 0	depth = 1"	depth = 2"	depth = 3"	depth = 5"	depth = 6"	depth = 12"
20-mm round	3.53	1.70	2.26	-2.27	------	------	------	------
30-mm projectile	7.9	1.81	3.87	------	2.85	------	------	------
100 g C4	34	5.31	------	3.22	3.16	------	2.08	------
200 g C4	68	------	------	3.39	------	1.767	1.34	2.02
60-mm mortar	111.1	------	------	3.62	------	------	2.98	3.31
105-mm projectile	609.3	------	------	8.77	------	------	5.98	4.97

Table III-3. Values Obtained from Minimizing the Error as Defined in Eq. (3.15)

	C	B	α	β
Yuma	0.42	0.387	0.322	0.094
Socorro	0.59	0.151	0.085	1.826

We note that we have not applied any weights to each of the *i* terms in the sum in Eq. (3.15). A weighting function that accounts for the fact that each average value given in Tables III-1 and III-2 represents an average over a different number of data points could be incorporated. For example, the number of 81-mm shells at 2 in. does not equal the number of 105-mm shells at 6 in. One could also define a weighting function as the inverse of the

standard deviation of each average. Although one might expect these two factors to be correlated, it turns out that the smallest standard deviations do not correspond to those averages with the largest number of data points, nor do the largest standard deviations correspond to those averages with the smallest number of data points. For example, in the Yuma data set, there are five 40-mm shells at the surface: their average signal is 2.08 cpm, and the standard deviation is 1.1 cpm. On the other hand, there are eleven 81-mm shells at 2 in., with an average signal of 7.89 cpm and a standard deviation of 5.17 cpm. There are six 100 g simulants at 2 in. with an average signal of 2.62 cpm, and a standard deviation of 0.55 cpm, while there are twenty-two 60-mm shells at 2 in. with an average signal of 3.99 cpm and a standard deviation of 2.3 cpm. Because it was unclear what definition of the weighting function would be best, we decided not to include one in the present analysis; we note, however, that it may indeed prove useful to perform different fits using different weighting functions in future analyses.

We then used Eq. (3.15) with the values as given in Table III-3 to predict the signal for all 152 Yuma data points and 128 Socorro data points. Figures III-1 and III-2 show histograms of the absolute value of the difference between the predicted value and the measured value. Using $\sigma = 1.5$ cpm for the Yuma data and $\sigma = 2.4$ cpm for the Socorro data, we quantified the "goodness of fit" as shown in Table III-4.

Table III-3 shows that for the Yuma data, the value of β falls within the range predicted above in Section A. However, the Socorro data fits a value of β much larger than what we predicted. If we repeat our minimization on the Socorro data, holding the value of β fixed at a value of 0.09, the resulting values of B and α are 0.146 and 0.078, respectively. Interestingly, these values of B and α do not differ greatly from those shown in Table III-3, where β was a free parameter in the minimization. If the value of the error as defined in Eq. (3.15) is used as a measure of which values of B, α, and β yield the lowest minimum point, then the values given in Table III-3 are best. Specifically, the error for the values given in Table III-3 is 43.22 (recall that the sum is over 20 data points), while that for the case where β is held fixed at 0.09 is 56.47. To put this in perspective, the corresponding value for the Yuma data was 25.37 (sum over 27 data points). Figure III-3 shows a plot of the "difference histogram" corresponding to fixing $\beta = 0.09$ and the "goodness of fit" is displayed in the second-to-last column of Table III-4. In the last column of that table, we indicate the "goodness of fit" obtained if we use the Yuma values of B, α, and β for the Socorro data, keeping $C = 0.59$. (This last case yields a total error of 104.2.)

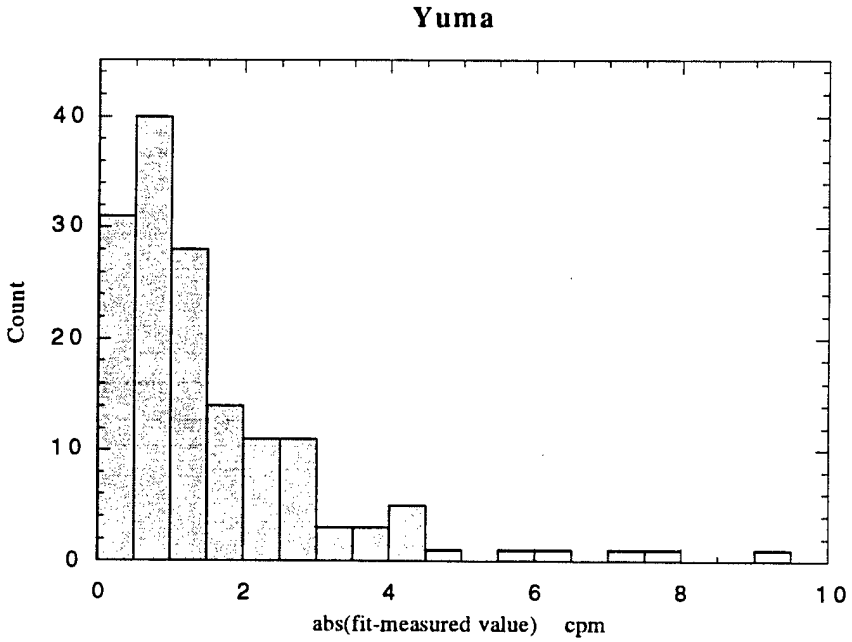

$$fit = 0.42 + 0.3872*M^{2/3}*(1-exp(-0.0937*M^{2/3}))*exp(-0.3224*depth)$$

Figure III-1. Yuma Data

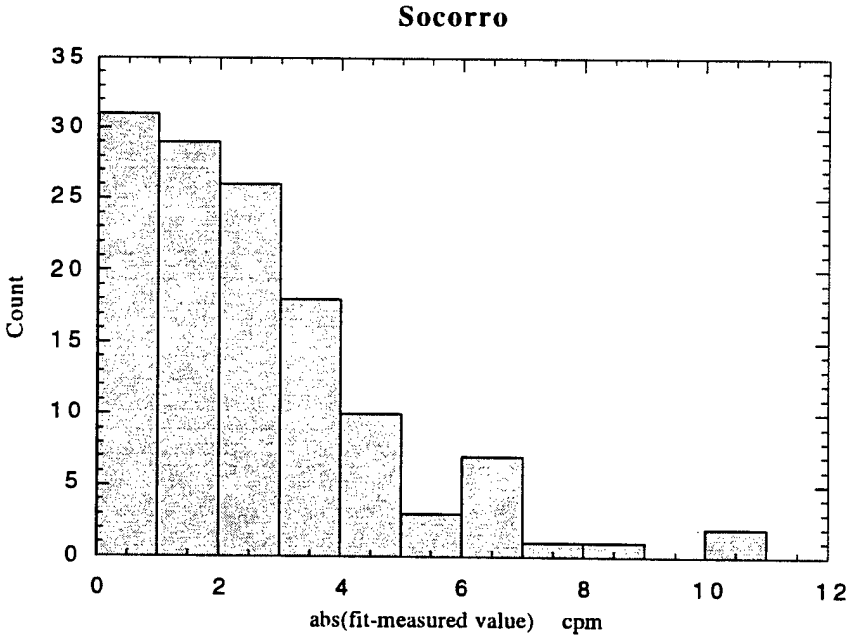

$$fit = 0.59 + 0.1507*M^{2/3}*(1-exp(-1.8258*M^{2/3}))*exp(-0.0851*depth)$$

Figure III-2. Socorro Data

Table III-4. Goodness of Fit

$\zeta \equiv$ abs (fit – measured signal)	Yuma data (152 total) $1\sigma = 1.5$ cpm	Socorro data (128 total) $1\sigma = 2.4$ cpm	Socorro data: fix $\beta = 0.09$ (128 total)	Socorro data: fit to Yuma parameters (keeping C = 0.59)
$0 \le \zeta \le 1\sigma$	99	74	73	71
$1\sigma < \zeta \le 2\sigma$	37	40	38	40
$2\sigma < \zeta \le 3\sigma$	10	10	13	11
$3\sigma < \zeta \le 4\sigma$	2	2	2	3
$4\sigma < \zeta \le 5\sigma$	2	2	2	1
$5\sigma < \zeta \le 6\sigma$	2	—	—	1
$6\sigma < \zeta \le 7\sigma$	—	—	—	1

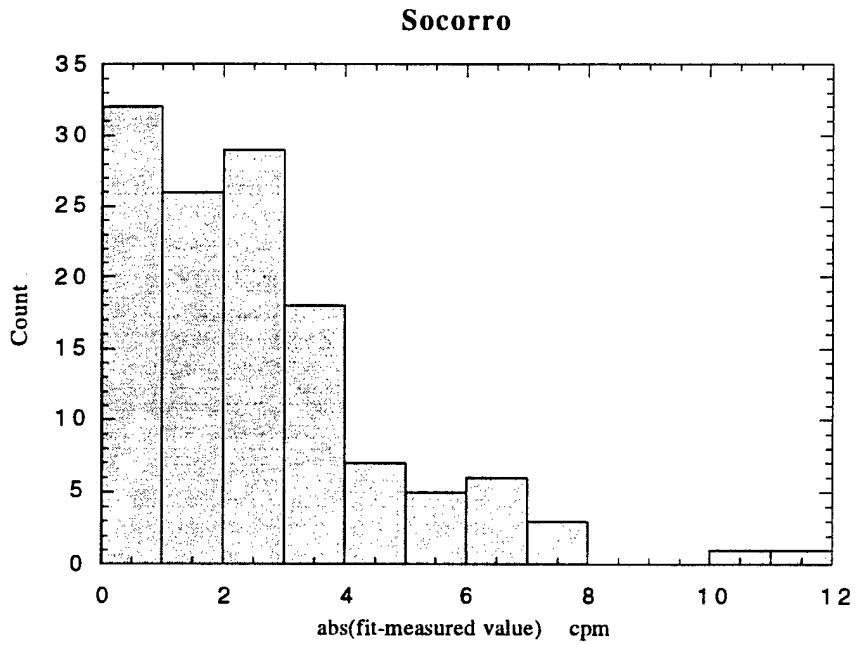

Figure III-3. Socorro Data Fit to $\beta = 0.09$

It is clear from Tables III-3 and III-4 that there was difference between the two sites. Particularly intriguing is the fact that the parameter B, which is a function primarily of the source intensity, varies by more than a factor of two between the two sites. As far as we are aware, the sources used at the two sites were very similar in strength, and hence, we find this difference somewhat puzzling. On the other hand, the cross-sectional area of the target also contributes to the value of B (see Section A above). Not only was our

treatment of this area very simplistic, but it is also possible that the orientations of the buried ordnance varied between the two sites such that the area term would differ significantly. Although a distribution of horizontal and vertical orientations was used at both sites, it is possible that the distributions differed or that there were correlations between the orientation and the ordnance type which varied between the two sites, or both. Appendix B gives another approach: combine the data at the two sites into one data set, and using Eq. (3.15), obtain a set of values for the parameters B, α, and β that best fit the combination data set. Appendix B also gives the result of fixing B and β for the Socorro to be equal to that of the Yuma data, and allowing only α to vary, since most of the site dependence should be tied up in α.

As a check on our model of the dependence on the mass, we repeated the minimization using the following definition of the error:

$$\text{error} \equiv \sum_{i=1}^{N} \left[(C + BM_i e^{-\alpha * \text{depth}_i}) - S_i \right]^2 \quad , \tag{3.16}$$

with the mass dependence given in Eq. (3.12). For the Yuma data, B = 0.055 and α = 0.367; for the Socorro data, B = 0.017 and α = 0.0756.

Figures III-4 and III-5 are histograms of the absolute values of the difference between the values predicted using Eq. (3.12) with these parameters and the measured values. Table III-5 gives the "goodness of fit." Comparing Tables III-4 and III-5, it is clear that Eq. (3.10) is preferable in describing the dependence of the signal on the mass, particularly in the case of the Yuma data. For the Socorro data, the difference is not as pronounced, probably because there were fewer masses tested at Socorro, and only one large mass was utilized. Because the effect is most pronounced at large masses, the results from Socorro regarding the mass dependence are a little more uncertain.

Although Eq. (3.10) better describes the signal dependence on the mass overall, Eq. (3.12) may be a better model for the smaller UXO, because for small objects, our estimate of the total path length of the neutrons in the target is too large [i.e., for small targets, the scattering mean free path is of the same order as, rather than significantly less than, the linear dimension of the target; see discussion preceding Eq. (3.9)]. Our model predicts a signal dependence of $M^{4/3}$ for small masses, rather than a linear dependence. On the other hand, the total number of data points involved in the utilization of Eq. (3.16) for the smaller masses would be small: only the 20-mm and 30-mm targets would most likely be considered. Furthermore, of the 16 targets at Yuma with signals greater than 2σ away

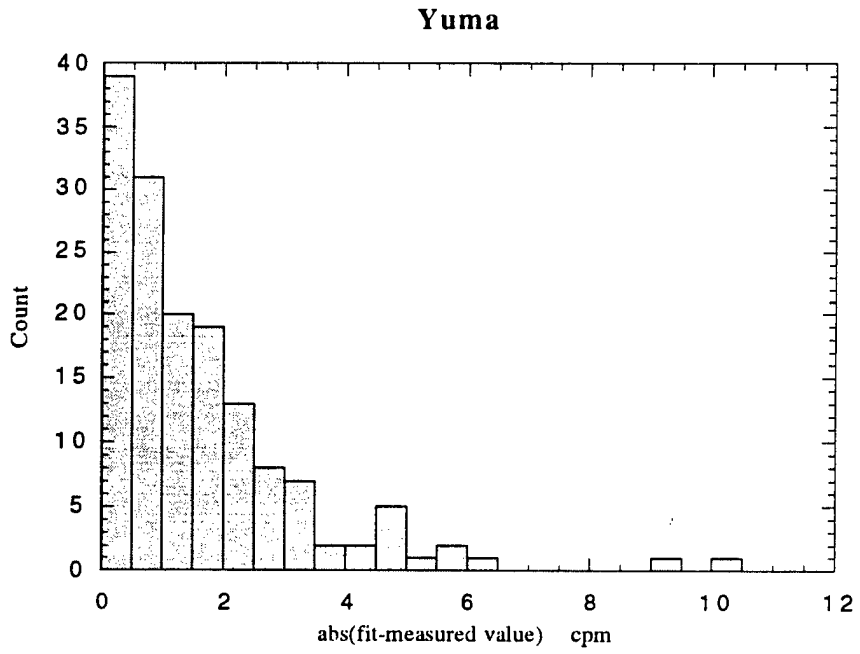

fit = 0.42 + 0.0550*M*exp(-0.3668*depth)

Figure III-4. Yuma Data Fit to Linear Mass Dependence

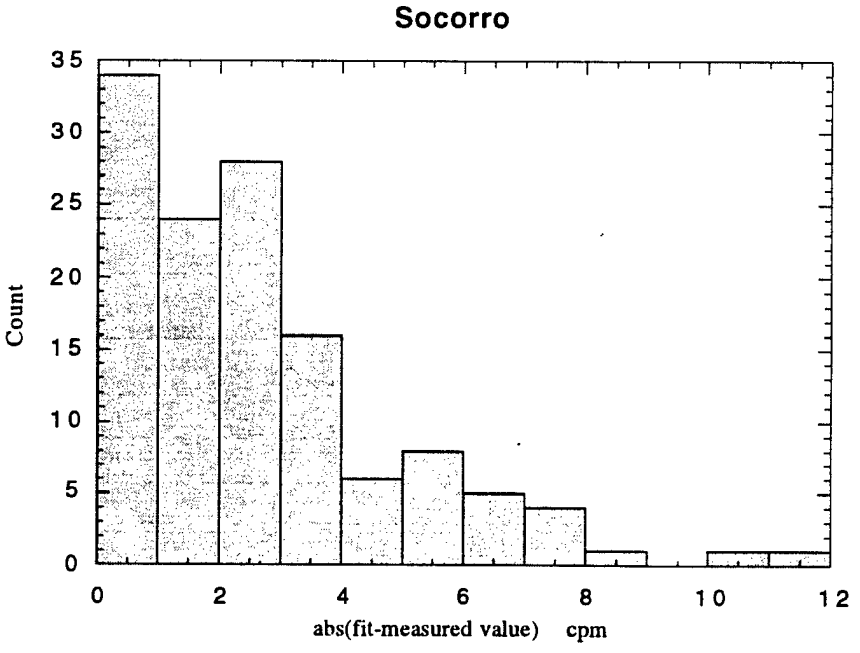

fit = 0.59 + 0.0170*M*exp(-0.0756*depth)

Figure III-5. Socorro Data Fit to Linear Mass Dependence

Table III-5. Goodness of Fit Using Linear Dependence on Mass

$\zeta \equiv$ abs (fit – measured signal)	Yuma data	Socorro data
$0 \le \zeta \le 1\sigma$	90	73
$1\sigma < \zeta \le 2\sigma$	41	35
$2\sigma < \zeta \le 3\sigma$	10	16
$3\sigma < \zeta \le 4\sigma$	8	2
$4\sigma < \zeta \le 5\sigma$	1	2
$5\sigma < \zeta \le 6\sigma$	0	—
$6\sigma < \zeta \le 7\sigma$	2	—

from that predicted by Eq. (3.14) and Table III-3, none are 20-mm or 30-mm targets. For the Socorro data, one of the two targets with signals that differed from the predicted values by more than 4σ is indeed a 30 mm, but the remaining 16 targets with signals greater than 2σ away from the predicted values are neither 20 mm nor 30 mm. Nonetheless, a model which incorporates two fits, depending on the mass of the object, is probably worth further investigation.

Finally, we examine the contribution of the $Si^{29}(n,\gamma)$ reaction to the background (reported by SAIC to be 60 cpm) to further explore the "goodness" of our fits. In Section A above, we postulated that

$$\frac{\text{cpm}}{\text{detector}} = \frac{I_0 e^{-\alpha^* \text{depth}} A_{\text{target}} N\sigma_{(n,\gamma)}}{\Sigma_{\text{tot-abs}}}\left[1 - e^{-\beta M^{2/3}}\right] + C \quad , \tag{3.17}$$

where cpm is counts-per-minute, A_{target} is the area of the target, I_0 is the neutron flux incident on the soil, $N\sigma_{(n,\gamma)}$ is the macroscopic cross section for the $N^{14}(n,\gamma\text{-to-ground})$ reaction in the target, and $\Sigma_{tot\text{-}abs}$ is the total macroscopic cross section for neutron absorption in the target. Using Eq. (3.17) and the fit to the Yuma data,

$$I_0\left(\frac{3}{\rho_{\text{exp}}}\right)^{2/3} \frac{N\sigma_{(n,\gamma)}}{\Sigma_{\text{tot-abs}}} = 0.3872 \frac{\text{cpm}}{g^{2/3}} \quad . \tag{3.18}$$

Using RDX as the representative explosive, $I_0 = 55$ cpm/cm^2.

To estimate the contribution to the background from Si^{29},

$$\frac{\text{cpm}}{\text{detector}} = I_0 A_{\text{tot}} \left(N\sigma_{(n,\gamma)}\right)_{Si^{29}} \int_0^{\infty} e^{-\alpha^* \text{depth}} , \tag{3.19}$$

where A_{tot} refers to the total irradiated area seen by the detector, and $N\sigma_{(n,\gamma)}$ is the macroscopic cross section for the Si^{29}(n,γ-to-ground) reaction (= 0.0077 b). The radius of the TNA system is about 35 cm, and we estimate that Si^{29} contributes about 8.4 cpm/ detector. This is about a factor of seven below the value given by SAIC, which seems reasonable, given the level of approximations used in our simple model. A similar calculation using the fits to the Socorro data gives an estimate of 12 cpm/detector. Finally, we have done a similar estimate using the Yuma data and Eq. (3.13b) for the signal dependence on depth. We obtain the same value given above (8.3 cpm/detector).

C. COMPARISON OF PERFORMANCE AT YUMA AND SOCORRO

SAIC upgraded the system for the Yuma test by adding four more NaI detectors (bringing the total to 12), and by increasing the measurement time from 5 to 10 minutes. One would expect, therefore, a decrease in statistical uncertainty in the Yuma data relative to the Socorro data of $\sqrt{(5\cdot 8)/(12\cdot 10)} = \sqrt{1/3}$, and hence, an improvement in performance.

To examine the true improvement in performance, we have calculated the probability of detection, P_d, versus the probability of false alarm, P_{FA}, for the two sites. Figure III-6 shows the curves.[4] Such curves are often referred to as receiver-operator characteristic (ROC) curves. We note, however, that the traditional ROC curve is determined solely by the system and will not vary from site to site. Curves generated for UXO detection systems, however, will almost always vary from site to site because both P_d and P_{FA} depend upon site conditions. Thus, the curves presented in Figure III-6 present information not only about the inherent improvement in the system due to the longer counting times and larger number of detectors, but also about differences between the two sites.

---

[4] As discussed in Section B above, the Yuma data set consists of 152 UXO from data collection and blind tests as sell as 2 inerts and 90 soil measurements. The Socorro data set consists of 128 UXO from data collection and blind tests and 60 inerts.

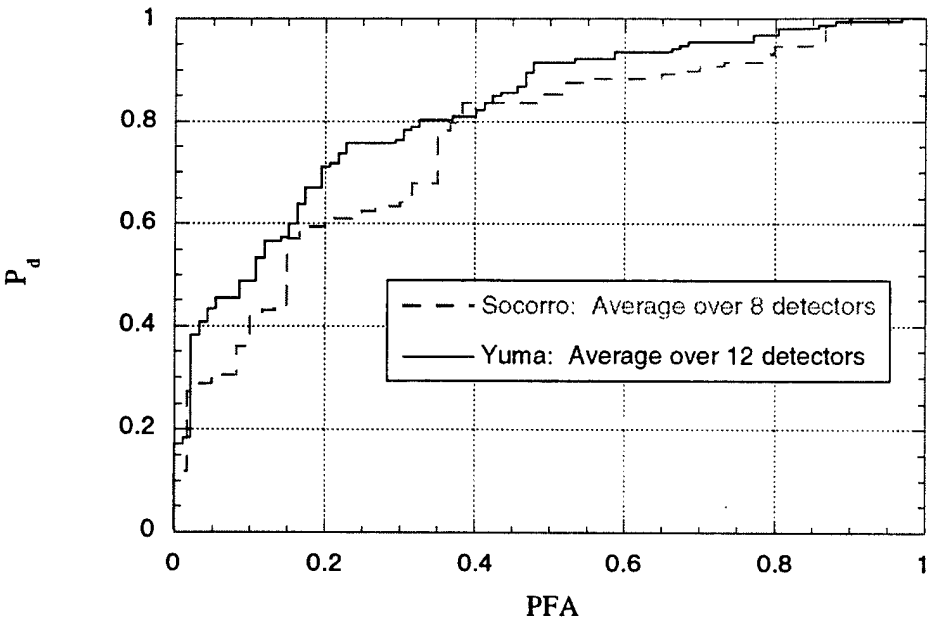

Figure III-6. ROC Curves of Performance at Yuma and Socorro

We note that for the Yuma data, SAIC actually employed two different detection algorithms. One of them involved comparing the average of the signal over the 12 detectors to a threshold, which they chose to be 1.5 counts per minute. Their second algorithm involved a logical "OR": if the average of the signal over the 12 detectors exceeded 1.5 counts per minute, OR if the average of the three largest signals from adjacent detectors exceeded a higher threshold (chosen to be 3.75 counts per minute), then a detection was declared. In the SAIC final report, the former algorithm is referred to as "real-time processing," while the latter is called "post-processing." While it is true that the latter method improves the probability of detection, it also increases the probability of false alarms. For the thresholds chosen, SAIC picked up an additional 17 targets using their logical OR approach, but they also doubled the number of false alarms. That is, the P_d for their real-time algorithm was 0.72 and the P_{FA} was 0.22, but the P_d for their post-processed algorithm was 0.83 and the P_{FA} was 0.43. There was virtually no improvement in system performance using the logical OR. We believe that this is related to the fact, discussed above in Section A, that there appears to be no correlation between signal strength and offset distance. Figure III-6 shows the ROC curve corresponding to the real-time detection scheme.

Based on the ROC curves, the system performed better at Yuma; however, even setting the threshold to 0.0 cpm would not yield 100-percent detection at either site.[5] The "zero-threshold" point occurs at $P_d = 0.93$ and $P_{FA} = 0.59$ for Yuma and at $P_d = 0.88$ and $P_{FA} = 0.56$ for Socorro (see Table III-6).

Table III-6. SAIC Results

Site	P_d	P_{FA}	Threshold cpm	Number of Detectors	Measurement Time (min)
Socorro	0.54	0.15	2.85	8	5
Yuma	0.72	0.22	1.5	12	10
Yuma post-processing	0.83	0.43	See text	12	10
Socorro	0.88	0.56	0.0	8	5
Yuma	0.93	0.59	0.0	12	10

We use our semi-empirical fits from Section B to further compare the performance at the two sites. Using Eq. (3.14) and Table III-3, we can answer the question, "For a given signal X and a given mass M, what depth do we predict?" Figure III-7a shows the results for X = 1.0, 1.5, 2.0, 2.5, and 3.0 cpm for the Yuma data, while Figure III-7b shows the same results for the Socorro data. It is clear from the figures that no matter how large the mass of the UXO, there is limit to the depth at which it can be detected. At Yuma this maximum depth is seen to be about 12 in., while at Socorro it approaches 40 in. On the other hand, our theory predicts better detection of smaller masses (at shallow depths) at Yuma than at Socorro, for thresholds equal to or exceeding 1.5 cpm. This conclusion is drawn with caution, however, because as noted above, our prediction for small masses overestimates the path length of neutrons in the UXO, and thus overestimates the signal at a given depth for small masses (i.e., it predicts that the signal strength is proportional to $M^{4/3}$ rather than to M).

5 Here, by zero threshold, we mean *after* the background subtraction is applied.

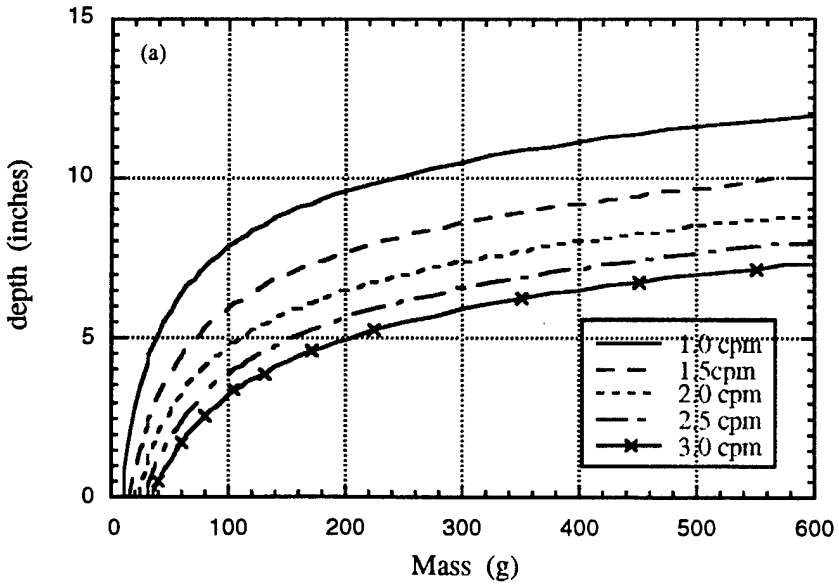

Figure III-7a. Performance at Yuma Based on Semi-Empirical Model

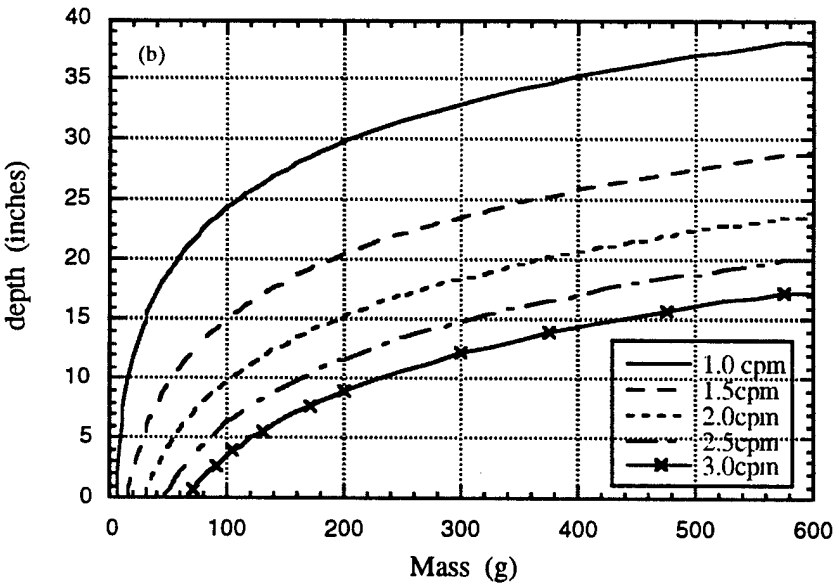

Figure III-7b. Performance at Socorro Based on Semi-Empirical Model

IV. HARDWARE ISSUES AND PROSPECTS FOR FUTURE IMPROVEMENTS

The signal-to-noise ratio of the current SAIC TNA system is of order unity, a value that is about an order of magnitude too low to be viable as a UXO detection system. Significant performance improvement may be attainable with hardware upgrades. We consider three such upgrades. In Section A, we compare scintillators and semiconductor detectors, and in Section B, we compare the current continuous fission source with a pulsed source. In Section C, we give estimates for the potential improvement in the system's performance if high-purity germanium (HPGe) detectors, a pulsed source, or both are utilized.

A. DETECTORS

The success of TNA as an approach to detect buried explosives is inextricably tied to the quality of the detectors. The ideal detector would have a high atomic number and density for high detection efficiency, a large size for high energy absorption and good spectral quality, and good energy resolution. In addition, the detector must be rugged for field use.

The most common γ-ray detectors fall into two categories: semiconductors and scintillators. A scintillation detector takes advantage of the characteristic of certain materials to emit a flash of light (i.e., a scintillation) when struck by radiation. When coupled to an amplifying device such as a photomultiplier tube (PMT), these scintillations are converted into electrical pulses, which then are analyzed and counted electronically to give information concerning the incident radiation. A good scintillator should possess several characteristics: (1) it should have a high efficiency, defined as the fraction of the energy deposited by the radiation that is converted into visible light; (2) the luminescence should be rapid, so that pulses are generated quickly and high count rates can be resolved without severe pile-up; (3) it should be transparent to self emission; and (4) the photons it produces should couple well with the photomultiplier tube.

The most common scintillator used for γ-ray detection is a NaI crystal doped with thallium (to make it transparent to self emission). It has the highest emission intensity and

therefore exhibits good signal-to-noise characteristics. In fact, the efficiency of all γ-ray detectors is commonly measured relative to that of a NaI detector. A detector with 100-percent relative efficiency (RE) has the same efficiency as a 3 × 3 NaI detector at the Co^{60} line (1.33 MeV).

Other possible scintillator candidates are bismuth germanate ($Bi_2Ge_3O_{12}$, or BGO) and cerium-doped rare-earth oxyorthosilicates [$Re_2(SiO_4)O$, where Re = Gd, Lu, and Y]. BGO has a much higher Z than NaI(Tl), and therefore a higher detection efficiency, but about twice the line width of NaI(Tl). The rare-earth oxyorthosilicates have high density and average atomic number, reasonably high scintillation emission intensities (though lower than NaI), and fast scintillation decay times. $Gd_2(SiO_4)O$, or GSO, has had limited application in oil-well logging and PET (positron emission tomography), and has been in use in field measurements for almost 10 years. $Lu_2(SiO_4)O$, or LSO, has been commercially available for only about 1 year. A summary of the relevant characteristics of four major scintillators is given in Table IV-1.

Table IV-1. Scintillator Characteristics

	NaI(Tl)	BGO	GSO $Gd_2(SiO_4)O$:Ce	LSO $Lu_2(SiO_4)O$:Ce
Relative emission intensity	100	15	25	75
Decay constant (ns)	230	300	60	40
Density (g/cc)	3.67	7.13	6.7	7.4
Effective Z	51	75	59	66

The greatest drawback of a scintillation detector is that, in general, scintillators have a W value (energy expended by the incident radiation to produce a photoelectron at the cathode of the PMT) of several hundred eV/photoelectron, which leads to an energy resolution significantly poorer than that of semiconductors. (Although the energy resolution of a detector depends on other factors as well, the relatively large value of W for scintillators yields poor statistical resolution of the energy peak.) The poor energy resolution of NaI detectors is the greatest limitation in the current design of the SAIC TNA system, because the 10.6-MeV γ-ray resulting from the $Si^{29}(n,\gamma)$ reaction is not resolved from the N^{14} 10.8-MeV peak. Consequently, a complicated background subtraction procedure is employed.

A semiconductor detector is essentially a reverse-biased p-n junction. The depletion region, which is the active volume, has high resistivity, and carriers produced there by radiation can be collected swiftly and efficiently. In contrast to scintillation detectors, the W values for semiconductors are typically only a few eV/ion pair. The energy resolution is therefore greatly improved over that of a scintillation detector.

The most commonly used semiconductor detector today is high-purity germanium (HPGe) which provides excellent energy resolution. However, until 10 years ago, the size of a detector-quality Ge crystal that could be grown was severely limited. A small size implies that many of the incident photons escape after undergoing one or more Compton scattering interactions. Thus, the spectra would commonly exhibit extensive Compton continua, which tended to obscure low-intensity photopeaks. In addition, a small size implies poor energy collection efficiency, leading to very long measurement times to achieve adequate statistical precision. Thus, the improvement one would gain in energy resolution would be offset by a decrease in detection efficiency. Based on the technology of 10 years ago, one would be hard pressed to argue for the use of Ge detectors in this application, since the measurement times needed to achieve good counting statistics at 10.8 MeV would be prohibitively long.

Today, however, HPGe detectors can be built with relative efficiencies (RE) in excess of 100 percent. The first 150-percent RE Ge detectors were built over 5 years ago. In fact, in the 10 MeV energy range of interest for this application, the efficiencies will be greater than those quoted at 1.33 MeV, because the stopping power of Ge is better than that of NaI due to its higher mass density. A 100-percent RE Ge detector would actually have about 130-percent efficiency at 10 MeV, relative to a 3 × 3 NaI detector.[6] Ultimately, the efficiency that can be expected from a Ge detector correlates with cost: a 50-percent RE radiation-damage-resistant Ge detector will cost about $50K; 100-percent RE will cost about $100 K. (These prices, however, are dictated by market-value and could be considerably less.) We note that it is better to purchase one 100-percent RE detector rather than two 50-percent RE detectors, because the larger the detector, the greater the capability to discriminate a full energy peak in a complex spectrum, because the peak-to-Compton ratio increases with increasing relative efficiency.

---

6 The estimate of 130-percent relative efficiency at 10 MeV was provided by EG&G Ortec. We note that few, if any, efficiency measurements have actually been made at 10 MeV.

In addition to cost, there remain other concerns associated with the field use of HPGe detectors. Detectors must be kept at temperatures near the liquid nitrogen temperature.[7] The use of liquid nitrogen for cooling requires that the detectors be well shielded from the source to prevent spurious nitrogen signals from the liquid nitrogen. A better approach would probably entail the use of electromechanical coolers, which weigh about 20 kg, and which can cool a detector down to liquid nitrogen temperature. The issue is again one of cost: these refrigerators cost about $20 K, considerably more than a dewar.

A second concern is microphonics, in which motions in the field translate into electrical noise at the input of the detector electronics. This noise is added to the signal from the detector, resulting in a loss of energy resolution. There are two possible sources of microphonics: (1) vibration of the crystal, which is biased at a few kV, can induce a transient electric field which looks like a signal at the electronics input, and (2) vibration of the high-voltage wire connections coupling the crystal to the electronics can induce noise. This problem is usually circumvented by tuning the detector for the specific application by analyzing the frequency response of the system in the given environment. In the case of TNA, where the concern is primarily with detecting high-energy γ-rays, some additional improvement may be possible if thicker materials (such as thick aluminum or stainless steel) are used on the end-cap of the detector to make it more rigid. (This cannot be done for low-energy applications where the end-cap must be thin enough for the radiation to penetrate.) [8]

One final concern in using Ge detectors is radiation damage. For this application, an n-type, rather than p-type, Ge detector should be chosen to provide a measure of resistance to neutron damage. In a p-type Ge detector, the outer contact is positively biased, which means that hole collection dominates the charge collection process; in contrast, for an n-type Ge detector, electron collection is the dominant process. Fast neutrons generate hole-trapping centers; that is, negatively charged defects that trap holes but not electrons. Thus, the n-type detector, in which the hole collection process is of secondary importance, is less sensitive to neutron radiation damage than the p-type detector.

---

7 The limiting operating temperature is actually higher than liquid nitrogen temperature and is about 100 K.

8 The end cap is not the most important detector component as far as microphonics is concerned, but stiffening it should help somewhat.

B. NEUTRON SOURCES

A second hardware issue concerns the source of neutrons. The current system employs an isotopic fission source (Cf^{252}). Such sources are fairly inexpensive[9] and reliable. However, they do require constant shielding, and because the source is decaying there will be a (gradual) loss of source strength with time. Furthermore, with a continuous neutron source, one has no way to eliminate unwanted contributions to the γ-ray spectrum from fast neutrons, which contribute to the background in two ways: (1) fast neutrons can produce high energy γ-rays in the window of interest from interactions with atoms in both the soil and in the detector, and (2) fast neutrons can produce lower energy γ-rays which still contribute to the background in the window of interest through pulse pile-up.

In addition to these contributions to the statistical error, fast neutrons also contribute to the "systematic" error due to the background subtraction algorithm. This algorithm essentially involves several "pure soil" measurements (i.e., no explosives present). The ratio of counts in the low-energy part of the spectra to those of the high-energy part of the spectra is determined. Then, when measurements are made in an area where explosives might be present, the counts are determined in the low-energy part of the spectra, where the statistics are good, and the number of background counts in the high energy window are estimated using the ratios determined from the "pure soil" measurements. Fast neutrons degrade the performance of this background subtraction algorithm by contributing γ-ray counts over the entire energy spectrum, thereby worsening the correlation between the high-energy region background and the low-energy region.

The main reason to change to a pulsed source from the current fission source would be to eliminate the fast neutron interactions. A pulsed source allows one to gate out the fast neutron interactions. The fast neutron interactions decay in about 50 μs, whereas the thermal neutron interactions decay away in about 1 ms. If a pulsed source is turned on for a few microseconds, turned off, and if there is a 100–150 μs delay before measurements are taken, the spectra obtained will be due to thermal neutron interactions only. Because pulsed sources are more costly, have a shorter lifetime, and may require significant moderation (see discussion below), the question is whether the removal of fast neutron contributions to the spectrum generated by the current fission source is worth the effort.

---

[9] Although the purchase price of a fission source is quite reasonable, there are other costs to consider. In addition to the required shielding, there are costs associated with acquiring a license to use a radioactive source, paperwork processing every time the source must be shipped, and disposal costs, which can be greater than the purchase price.

1. Fast Neutron Interactions

The fast neutron interactions that produce γ-rays are of two types: fast neutron capture and inelastic scattering [often referred to as (n,n') interactions]. Inelastic scattering always involves a threshold energy that depends upon the energy level structure of the target nucleus (i.e., the neutron must have enough energy to excite the target nucleus to a higher energy level). For example, a fast neutron must have an energy of at least 6.43 MeV to have an inelastic scattering collision with O^{16}. Of course, even if the neutron has sufficient energy to undergo an inelastic collision, that is not the only possible outcome. For example, for neutron energies between 7 and 8 MeV, the cross section for inelastic scattering off O^{16} varies between 0.075 and 0.43 b, while for elastic scattering, it varies between 0.7 and 1.2 b. Fast neutron capture, on the other hand, has no threshold, but because of the 1/v behavior of the neutron capture cross section (described in Chapter II), the cross sections for fast neutron capture on most nuclei are very small. (For most nuclei, fast neutron capture cross sections for neutrons with energies of one to a few MeV range from 0.1 to 3 mb.)

Like all fission sources, the Cf^{252} source produces neutrons with an energy spectrum peaked at a little less than 1 MeV. Although the spectrum does have a high-energy tail extending out to about 20 MeV, most of the neutrons produced have energies less than 6 MeV, and the average neutron energy will be about 2 MeV.[10] For a fission source, the dominant fast neutron reaction for producing high-energy γ-rays of order 10 MeV is therefore fast neutron capture, because most neutrons will not have enough energy to produce (n,n') reactions yielding 10-MeV γ-rays. The most important fast neutron capture reaction will be that of capture on the iodine in the NaI detectors.[11] Neutrons with energies between 3 and 4 MeV, for example, will produce γ-rays with energies between 9.8 and 10.8 MeV due to capture off of I^{127}. The cross section for this interaction at these energies, although much greater than that of most fast neutron capture cross sections, is only about 0.07 b. This small cross section, combined with the fairly low number of neutrons with energies exceeding 3 MeV, implies that the contribution of high-energy γ-rays to the background from fast neutrons from a fission source is fairly

---

[10] Furthermore, SAIC employs a moderator which reduces the average neutron energy leaving the system to about 1 MeV.

[11] Although the detectors are shielded, some fast neutrons will penetrate.

small; SAIC estimates the number to be about 10 percent of the total background counts in the 10-MeV window of interest (about 9.6–11.0 MeV).[12]

As mentioned above, low-energy γ-rays produced by fast neutron interactions can also contribute counts in the window of interest through pulse pile-up. Pulse pile-up results when two or more pulses occur within the resolving time of the detector, such that they are treated as if they were one pulse. This composite pulse is then added to memory in a channel corresponding to the sum of the pulse heights that produced it. In addition to increasing the background, pileup can also decrease the signal: any γ-ray pulse may pile up with the 10.8 MeV pulse of interest, and the total energy will appear at higher energy (i.e., that signal will be lost).

Pile-up is a problem for all detectors to varying degrees, depending on the resolving time of the detection system. For scintillators, the resolving time is related to the decay time of the scintillator. As seen in Table IV-1, LSO and GSO have decay constants significantly shorter than those of NaI and BGO. For HPGe, the resolving time is dependent on the mobility of the electrons/holes in the Ge and the geometry and size of the detector. (The farther the charges have to travel, the longer the resolving time.)[13]

Pile-up is a function of the count rate (the higher the count rate, the more severe the pile-up) as well as the spectral shape (a large number of high-energy γ-rays will result in a higher pile-up in the 10.8 MeV region compared to a spectrum with the same total count rate and a lower number of counts in the high-energy region). Thus, for fast neutrons to contribute significantly to pulse pile-up, the γ-ray count rate due to fast neutron interactions must be high, and the γ-rays produced should have energies skewed toward high energies.

As explained above, fast neutron capture cross-sections are very small, so the dominant fast neutron contribution to pile-up will be inelastic scattering off of nuclei in the detector and in the soil. The most abundant nuclei in soil are silicon and oxygen, but the inelastic scattering threshold of oxygen is too high to be of interest for a fission source.

---

12 Capture on Na^{23} will also produce high-energy γ-rays; specifically, 2.6–4 MeV neutrons will yield γ-rays with energies between 9.6 and 11.0 MeV. However, the fast neutron capture cross-section on Na^{23} is only about 226 μb, about 400 times smaller than that of I^{127}. Fast neutron capture cross sections for soil nuclei are also much less than those of iodine.

13 For all detection systems, the time resolution can be improved at the expense of energy resolution. For example, the current SAIC system clips the pulse at 200 ns, which means that it is integrating over less than half of all the photons. Similarly, the pulse-width can be narrowed in a Ge detector such that the time resolution can be as good as about 15 ns. Ultimately, detailed optimization calculations are required to determine how much energy resolution can be sacrificed to reduce pile-up.

The threshold for natural Si is about 1.3 MeV, corresponding to the first excited state of Si^{29}, a value that is slightly greater than the average neutron energy entering the soil.[14] However, the cross section for this reaction in natural silicon is very low, with a maximum value of only 0.02 b, because natural silicon contains only 4.67 percent Si^{29}. The only Si (n,n') reaction with a significant cross section in natural silicon is the one that excites Si^{28} to its first energy level; it has a threshold of 1.84 MeV and a cross section that ranges from 0.1–0.9 b for neutrons with energies between 2 and 6 MeV. Hence, inelastic scattering from Si will only be relevant for neutrons with energies greater than about 2 MeV. We note, however, that even those neutrons with energies greater than 2 MeV will not necessarily scatter inelastically off of Si; for neutron energies between 2 and 6 MeV, the elastic scattering cross section for Si ranges from 1 to 3 b, and that of oxygen ranges from 0.8 to 3 b. Thus, elastic scattering will slow many of the neutrons down below the threshold energy before they can scatter inelastically.

In order of abundance, other important nuclei in the soil are Al (8.2%), Fe (5.6%), Ca (4.2%), Mg (2.8%), Na (2.4%), and K (2.1%), with (n,n') thresholds of 0.87 MeV, 0.87 MeV, 1.2 MeV, 0.6 MeV, 0.46 MeV, and 2.6 MeV, respectively. Although some of these thresholds are below 1 MeV, only Na has a significant cross section below 1 MeV.[15] Furthermore, all of these nuclei have elastic cross sections exceeding the corresponding inelastic cross sections at neutron energies below 6 MeV.[16]

In the detector, inelastic scattering will occur off of both Na and I. The threshold for I(n,n') is only 0.06 MeV, and thus many more neutrons can participate in I(n,n') reactions. On the other hand, the maximum γ-ray energy produced in I(n,n') reactions is about 2 MeV. Furthermore, elastic scattering off Na in the detector will slow some of the

---

14 See Footnote 9.

15 For Na, $\sigma(n,n') \approx 0.24–0.5$ b for 0.6 MeV $< E_n <$ 1 MeV.

16 Specifically, the values for $\sigma(n,n):\sigma(n,n')$ for neutrons with fission spectrum average energies are about 10 for Al, 4 for Fe, 60 for Ca, 9 for Mg, 5 for Na, and 50 for K, according to the database provided by Brookhaven National Lab. Estimates for neutrons with energies between 1 and 6 MeV are as follows. For Al, $\sigma(n,n)$: $\sigma(n,n')$ is about 4–8 for 1.6 MeV $< E_n <$ 3 MeV, and is about 2–3 for 3 MeV$< E_n <$ 6 MeV; for Fe, this ratio is about 2–3 for 1 MeV $< E_n <$ 6 MeV ; for Ca, this ratio is about 250 for $E_n <$ 3.4 MeV, about 20 for 3.5 MeV $< E_n <$ 4 MeV, and about 4–10 for 4 MeV $< E_n <$ 6 MeV; for Mg, this ratio is about 3–6 for 1.6 MeV $< E_n <$ 3 MeV, and is about 2–3 for 3 MeV $< E_n <$ 6 MeV; for Na, this ratio is about 5–15 for 0.6 MeV$< E_n <$ 1 MeV, about 3–10 for 1 MeV $< E_n <$ 3 MeV, and is about 1–2 for 3 MeV $< E_n <$ 6 MeV; and for K, this ratio is about 40 for $E_n <$ 3 MeV, about 10 for 3 MeV $< E_n <$ 4 MeV, and about 4–8 for 4 MeV $< E_n <$ 6 MeV. These numbers were estimated from cross-sectional data provided by Brookhaven National Lab and are approximate; many of the inelastic cross sections exhibit a rich resonance structure.

neutrons down before they can inelastically scatter from Iodine.[17] We note that almost all of the (n,n') interactions that occur both in the soil and in the detectors will produce γ-rays with energies less than about 2 MeV.

Thus, we conclude that the contribution of fast neutrons to pulse pile-up is not significant for a fission source. The reason is simple: a fission source does not produce a significant number of neutrons with energies high enough to produce a large number of inelastic scatter γ-rays. Furthermore, not only is the count rate low, but the spectrum of γ-rays produced is skewed toward lower energies. For the current system, SAIC estimates that about 10 percent of the background in the 10-MeV window is due to pulse pile-up. Based on the above reasoning, the majority of those counts are due to thermal neutron capture off elements in the soil, rather than fast neutron interactions.

2. Fast Neutron Interactions and Systematic Error

We now consider the effect of fast neutron interactions on the systematic error introduced by the background subtraction algorithm. As with pulse pile-up, fast neutron capture will contribute only a small number of counts, given the small cross sections. On the other hand, inelastic scattering interactions will be more important than they were for pulse pile-up in the 10-MeV window, because the low energy γ-rays produced will be more important. Nonetheless, the total count rate due to fast neutron interactions is fairly small, for the reasons discussed above. Thus, although the effect of fast neutrons will be more substantial for the background subtraction algorithm than for pile-up in the 10-MeV window, the effect will still be lower than the contributions from thermal neutron capture off soil elements.

3. Other Issues for Pulsed Sources

Based on the above discussion, one would be hard-pressed to argue in favor of pulsed sources. It is likely that there will be some benefit, but overall, a pulsed source would do little to mitigate what is the primary source of error for this system: the Si background. Furthermore, there are other problems associated with pulsed sources. The most common pulsed source is a deuterium-tritium accelerator (called a D-T tube), commonly used in oil-well logging. These accelerators are fairly small and light, and typically accelerate with voltages of about 100 keV. However, they produce 14 MeV

---

[17] The elastic scattering cross section for Na ranges from 1.5 to 3 b for 1 MeV < E_n < 2 MeV and from 0.9 to 1.5 b for 2 MeV < E_n < 6 MeV.

neutrons, which implies a need for a significant increase in moderating material (and hence weight) over that used in the current system.[18] Furthermore, D-T tubes are more expensive than isotopic sources, and they have a limited lifetime of about 1,000 hours. On the other hand, they are safer from a radiological standpoint: unlike the Cf^{252} source, they can be turned off with the flick of a switch.[19]

A deuterium-deuterium (D-D) accelerator may be a better choice because it produces much lower energy neutrons (about 2.45 MeV), thereby requiring much less moderation than a D-T tube. However, the neutron production cross section for D-D reactions is about two orders of magnitude less than that for the D-T reaction, so getting enough counts and building a field-portable system would be important issues for a D-D accelerator source. A fairly large accelerator will be needed, implying a significant cost increase over an isotopic source.

Finally, we note that if a D-T accelerator were used, then it of course makes sense to pulse it. Unlike the fast neutrons from a Cf^{252} source, the fast neutrons from a bare D-T tube will contribute a significant amount to the total count rate. In fact, the contribution of fast neutron contributions to the total count rate may be as much as 10 times that of the thermal neutron interactions. Thus, pulsing a D-T source and gating the fast neutrons allows one to operate in a regime where the count rate, and hence the pile-up, is very low, compared to that of a continuous D-T source. On the other hand, it will probably not be necessary to pulse a D-D source, because the neutron energy will be low enough that significant inelastic scattering will not occur. In fact, unlike a Cf^{252} source, a D-D source will not have a high-energy tail, so the contribution of fast neutrons to the total count rate will be even lower than for the current Cf^{252} source.

C. ESTIMATE OF POSSIBLE IMPROVEMENTS DUE TO HARDWARE UPGRADES

Given that improvements in both detector and source technology will require a significant increase in cost, the question is whether such improvements are worth the investment. A detailed investigation is beyond the scope of this report; however, we will provide a semiquantitative analysis here.

---

[18] On the other hand, one might consider designing the system without a moderator and use the 14 MeV neutrons to probe deeper into the soil, relying on the moderation by the soil elements.

[19] The cost trade-off of using a neutron generator is more complicated than implied here. See Footnote 8.

In the current SAIC system, the background signal in the region of interest (9.6–11.0 MeV) is about 100 counts per minute (cpm). Of these counts, SAIC estimates that 60 are due to the Si 10.6 MeV line, 20 are due to cosmic rays, 10 are due to fast neutron reactions, and 10 are the result of pulse pile-up.

We begin with an estimate in the improvement in peformance that could reasonably be expected if the Cf^{252} continuous isotopic source were replaced with a pulsed source. As discussed above, pulsing a neutron source enables one to gate out fast neutron contributions. The spectra obtained therefore mimic those from a purely thermal source. Thus, we want to know how much improvement would result from changing from a fission source of neutrons to a purely thermal source.

Let us first consider the effect on the background count rate. If the strength of the pulsed source is such that the average thermal neutron intensity is roughly equivalent to that of the current source, then the contribution from the Si is basically unaffected.[20] The contribution from cosmic rays is also unaffected. The contribution from fast neutron capture in the detector should be eliminated. And finally, the contribution from pulse pile-up will be reduced only slightly. To be conservative, we will assume that the pile-up is essentially the same, and hence, the total reduction in background counts is only 10 percent.

The improvement will be better than this once we consider the background subtraction algorithm. Elimination of fast neutron interactions will improve the algorithm's performance somewhat. However, as discussed in Section B, because the energy spectrum of a fission source is such that most neutrons have energies below a few MeV, fast neutron contributions to the total count rate are low, and thus, the improvement in the background subtraction algorithm will probably be from 20 to 25 percent.

Let us now consider what would happen if we take the current SAIC system and change to HPGe detectors. To estimate the potential improvement in performance over NaI detectors, we need to know the time and energy resolution of the HPGe detector. These two parameters are not independent: one improves at the expense of the other. Assume 100-percent RE HPGe detectors, with an energy resolution of 20 keV at 10 MeV, a time response of 50 ns, and an energy window of 100 keV. The signal measured by the NaI detectors includes all three nitrogen peaks—the 10.8-MeV peak and the two escape peaks at

---

[20] This is an important point, because the thermal neutron intensity will decay exponentially for a pulsed source.

10.3 and 9.8 MeV. Thus, to maintain the same signal, we will look at three windows centered on those three escape peaks.

The contribution to the background signal from the Si line is now eliminated: we no longer have a problem distinguishing the N peak(s) from the Si peak(s). However, there will remain some background counts from nitrogen in the soil. (The 60 cpm actually includes contributions from both Si^{29} and N^{14} in the soil, but the Si^{29} contribution dominates. Only when the Si^{29} contributions are eliminated must one consider nitrogen.) We can estimate the N background using Eq. (3.19) in the data analysis section, where we have estimated the Si background using our semi-empirical model of the signal as a function of mass and depth. To use Eq. (3.19), we replace $(N\sigma_{(n,\gamma)})_{Si29}$ with $(N\sigma_{(n,\gamma)})_{N14}$, and because our prediction of the Si background is about seven times smaller than that reported by SAIC, we will multiply our result by seven. For dry soil, $(N\sigma_{(n,\gamma)})_{N14}$ is roughly 2.4×10^{-8} cm^{-1} (where we are considering only the γ-to-ground reaction). This leads to a prediction of only 0.275 cpm for sites like Yuma and Socorro. However, for soils with a significant amount of vegetation (forests, fields, farmland), the value of $(N\sigma_{(n,\gamma)})_{N14}$ can be as much as 20 times greater (i.e., 1 kg of N per m^3 of soil), leading to a background estimate of 5.5 cpm. To be conservative, we will use this value.[21] (We note that in reality, most of the naturally occurring nitrogen will be located near the surface, rather than uniformly distributed throughout the volume, so this estimate may not be that conservative.)

Let us now consider the other contributions to the background. The cosmic rays will be reduced from 20 cpm to $3 \times (100\ keV/1.4MeV) \times 20 \sim 4.3$ cpm. The fast neutron and pile-up contributions cannot be estimated easily, because these two factors are detector dependent. However, for our order-of-magnitude calculation, we estimate the pile up to be 10 cpm/ 1.4 MeV $\times$ (50/200), which gives 0.0018 cpm/keV. Multiply by 100 keV and by 3 windows, and we get about 0.5 cpm. Because fast neutron capture in the detector is the primary contributor to the fast neutron background, it is difficult to estimate the fast neutron contribution in HPGe detectors without knowing the details of the detector geometry,

---

21 An alternate way of estimating the nitrogen background would be to assume that the 60 cpm given by SAIC is uniformly distributed over the 1.4 MeV window. Then, for the case of 1 kg of N per m^3 of soil, the nitrogen background would be $[(N\sigma_{(n,\gamma\text{-to-ground})})_{N14} / (N\sigma_{(n,\gamma\text{- to-ground})})_{Si29}] \times (60/1.4$ MeV) = 0.0046 cpm/keV. Multiplying this number by 300 keV gives 1.4 cpm. However, this underestimates the nitrogen background, because the Si background is not uniformly distributed throughout the 1.4 MeV window (i.e., as the window shrinks to width ε centered on 10.8 MeV, the background N signal does not shrink to $0.0046 \times \varepsilon$ cpm).

shielding, etc. We ignore the differences between the two detectors for this contribution and take the fast neutron count rate to be 10×100 keV/1.4 MeV $\times$ 3 = 2.1 cpm.[22] Thus, the total background for HPGe is estimated to be about 12.4 cpm. To be conservative, we assume that the background count rate for an HPGe detector will be 15 cpm, a reduction of 85 percent over the NaI detectors.

We note that we have assumed 100-percent RE HPGe detectors, but as mentioned in Section A, an HPGe detector rated at 100-percent RE will actually have about 130 percent the efficiency of an NaI detector at 10 MeV. This implies that the total measurement time may actually be reduced from that of the current system by as much as 30 percent if 100-percent RE HPGe detectors are used. So, for example, the current system yields a total background of 1,000 counts per detector for a 10-minute measurement time. Replacing the NaI detectors with HPGe detectors could reduce this number to as low as 105 counts per detector, for a 7-minute measurement time. However, in reality, the increased cost of the HPGe detectors would mean that one would probably purchase far fewer than 12, so that the total system performance will not be improved as much as implied by these "per detector" numbers.

Finally, we consider the case where we use both HPGe detectors and a pulsed source. Again, assume that the average thermal neutron flux is roughly equivalent to that of the Cf^{252} source. Fast neutron interactions will again be eliminated, and pile-up will be only slightly affected. To be conservative, we assume that the only result is a reduction in fast neutron contributions, leading to a count rate per detector of about 13 cpm, with a total of 130 counts in 10 minutes. If one considers that the detectors will be operating at a true efficiency of 130 percent relative to NaI, then the measurement time will be only 7 minutes, leading to a total background of only about 90 counts per detector.

Table IV-2 gives a summary of this semi-quantitative comparison of different systems. We note again that a detailed analysis is well beyond the scope of this report. The numbers in the table are intended simply to provide the reader with a semi-quantitative understanding of the potential improvements from hardware upgrades. More accurate estimates can only be made from careful experiments.

---

22 This is probably conservative, because for NaI, most fast neutron capture contributions will occur at the lower end of the energy window, since for a Cf^{252} source, there are significantly more neutrons at 3 MeV than at 4 MeV.

Table IV-2. Potential Improvements With Hardware Upgrades

System	Background count rate per detector	Total background counts per detector	Systematic errors[†]
NaI detectors pulsed source with same average thermal yield as current Cf^{252} source	↓ by a little more than 10%	↓ by a little more than 10%	reduced by ≈ 20–25%[††].
100% RE HPGe detectors Cf^{252} source	↓ by factor of 6–7[*]	↓ by factor of 9–10[**]	essentially eliminated
100% RE HPGe detectors pulsed source with same average thermal yield as current Cf^{252} source	↓ by factor of 7–8[*]	↓ by factor of ≈11[**]	essentially eliminated

† It is assumed that the dominant contribution to the systematic errors comes from the background subtraction algorithm.

†† This number is very difficult to estimate. See text.

* Probably even greater reduction in dry soil. This number assumes 1 kg N/m^3 of soil, appropriate for forests or farmland.

** This number assumes that 100-percent RE HPGe detectors operate at about 130-percent RE at 10 MeV.

In conclusion, the best chance this system has to attain the order of magnitude improvements necessary to go from a proof-of-concept instrument to an employable UXO detection system is to use HPGe detectors. The reason is simple: the overwhelming source of error, both statistical and systematic, is the Si background. A pulsed source does not attack this problem directly; it could conceivably produce cleaner spectra and hence an improved subtraction algorithm, but the level of improvement would likely not be substantial enough. HPGe detectors, on the other hand, can theoretically eliminate the Si background problem altogether.

GLOSSARY

BGO	bismuth germanate
cpm	counts per minute
D-D	deuterium-deuterium
D-T	deuterium-tritium
ESTCP	Environmental Security Technology Certification Program
FUDS	formerly used defense sites
GSO	$Gd_2(SiO_4)O$
HPGe	high purity germanium
LSO	$Lu_2(SiO_4)O$
NVESD	Night Vision and Electronic Sensors Directorate
PET	positron emission tomography
PMT	photomultiplier tube
RE	relative efficiency
ROC	receiver-operator characteristic
S/N	signal to noise
SAIC	Science Applications International Corporation
TNA	thermal neutron activation
UXO	unexploded ordnance

APPENDIX A

THERMAL NEUTRON CAPTURE ON SELECTED NUCLEI

APPENDIX A
THERMAL NEUTRON CAPTURE ON SELECTED NUCLEI

THERMAL NEUTRON CAPTURE ON O^{16}

Oxygen is the most common element in the Earth's crust, with the mass 16 isotope being the most common. The binding energy of a neutron added to O^{16} is 4.14 MeV, a relatively low binding energy. (See energy level diagram for O^{17}, Fig. A-1) The thermal neutron capture on O^{16} is about 200 μb, a very small cross section. This can be understood by looking at the energy level diagram further. First, the nearest 1/2+ state in O^{17} is over 2 MeV away from the O^{16}+ thermal neutron energy. This leads to a very large energy denominator in the Breit-Wigner formula. The decay proceeds via electric dipole radiation through the 3.06 MeV state and magnetic dipole radiation through the 0.87 MeV state, with the electric dipole path favored by a little more than a factor of five. The preferred transition has a low energy (1.01 MeV), and as a result is relatively slow.

The low neutron capture cross section results from these two effects—a high off-resonance energy decreasing the compound nucleus formation and a low photon energy decreasing the gamma decay rate of the compound nucleus. This low cross section means that in typical soils even though oxygen is the most common component, it has, with a mean free path of about 750 m, a negligible effect on attenuating the neutron flux via capture.

THERMAL NEUTRON CAPTURE ON N^{14}

Nitrogen is the target nucleus used to indicate the presence of ordnance. The binding energy of an added neutron is 10.8 MeV, which is one of the highest values. (See energy level diagram for N^{15}, Fig. A-2.) This is what makes the signature promising for identification purposes—even though the nitrogen is rare, most common materials do not have such high energy γ rays produced by neutron capture. The (n,γ) cross section to the ground state, which gives off the distinctive 10.8 MeV γ is approximately 11 mb, or 50 times larger than the total capture cross section for oxygen. The total (n,γ) capture cross section is 77 mb, or about 350 times larger than that for oxygen. Even this relatively large cross section does not significantly attenuate the neutron flux over the distances of interest.

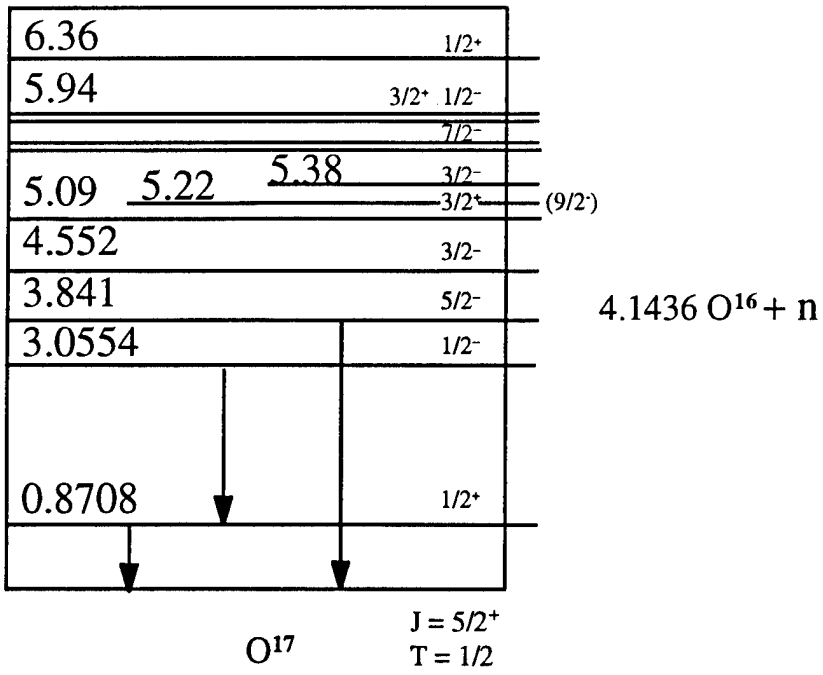

Figure A-1. Energy Level Diagram for O^{17}

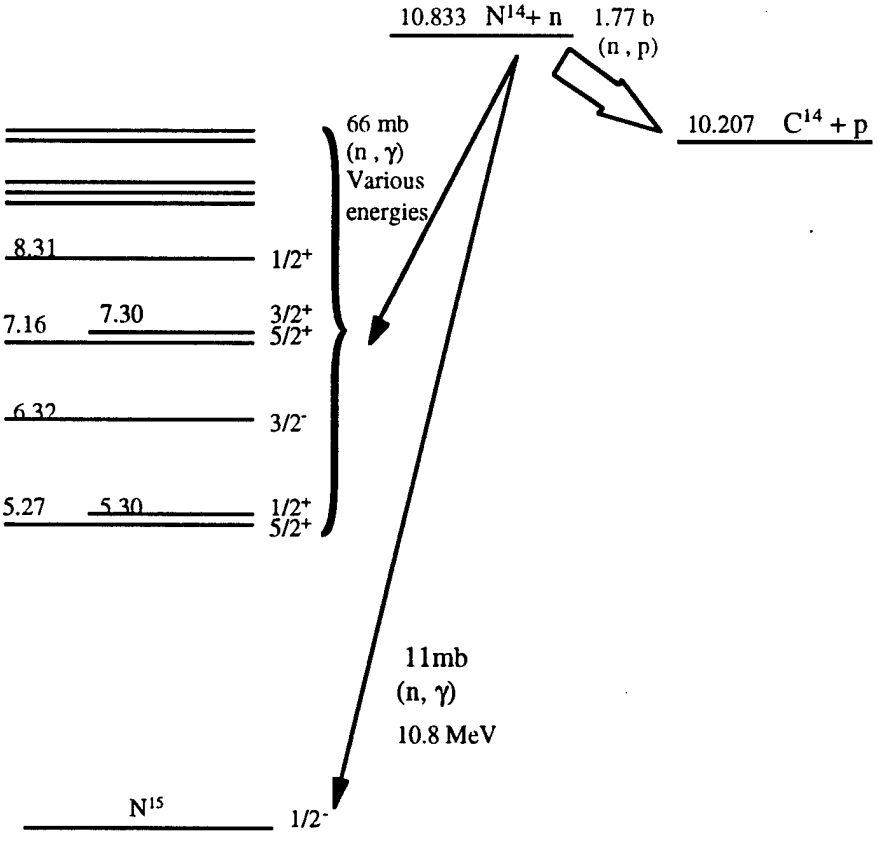

Figure A-2. Energy Level Diagram for N^{15}

However, the neutron capture on N^{14} is not dominated by the (n,γ) reaction but by the (n,p) reaction, which has a thermal cross section of 1.83 b. In typical soils, nitrogen does not a significantly attenuate neutrons because it is so rare—the capture cross section is 10,000 times larger, but the number density is 20,000 times lower. However, in concentrated amounts, such as in explosives, the nitrogen is a significant attenuator of the neutrons. A neutron slowed within typical explosive material in a shell will have a mean free path for capture of about 16 cm. This is large compared to most shells; however, because of the large scattering cross sections, the path length is long compared to the distance traveled. Hence, for medium or large shells there is a significant "self-screening" effect due to the N^{14} (n,p) reaction scavenging neutrons that would otherwise be available for (n,γ).

APPENDIX B

FURTHER ANALYSIS OF THE DATA

APPENDIX B
FURTHER ANALYSIS OF THE DATA

To further investigate the difference between the two sets of parameters obtained for the Yuma and Socorro data sets, we have combined the two data sets into one and obtained average values at each mass and depth (see Table B-1). The value of "C" in Eq. (3.14) was obtained from the combined inert/soil data from the two sites and was found to be 0.49 cpm. The standard deviation of the combined data set was 1.9 cpm. We have found that the values of B, α, and β which minimize the error function in Eq. (3.15) are 0.231, 0.166, and 1.08, respectively.

Following the procedure in Section III.B, we then used these values to predict the signal for all 280 UXO in our combined data set. Figure B-1 is a histogram of the absolute value of the difference between the predicted value and the measured value. Table B-2 shows the "goodness of fit." It is clear that the fit is not as good as the fits that were done separately for each site; nonetheless, one could argue that the fit is reasonably good.

Table B-1. Combined Data Set

Explosive Type	Nitrogen Mass (g)	depth = 0	depth = 1"	depth = 2"	depth = 3"	depth = 5"	depth = 6"	depth = 12"
20-mm round	3.53	1.35	2.07	-2.27	------	------	------	------
30-mm projectile	7.9	1.65	2.23	------	2.15		------	------
100 g C4	34	4.60	1.45	2.98	3.16	------	1.90	0.78
40-mm projectile	39.6	2.08	------	2.29	------	------	1.73	------
200 g C4	68	------	------	2.89	------	1.77	1.65	2.14
60-mm mortar	111.1	------	------	3.91	------	------	2.45	3.31
81-mm mortar	200	------	------	7.89	------	------	3.29	1.07
2.5 lb C4	378.3	------	------	11.98	------	------	4.29	1.60
105-mm projectile	609.3	------	------	10.04	------	------	5.47	4.33

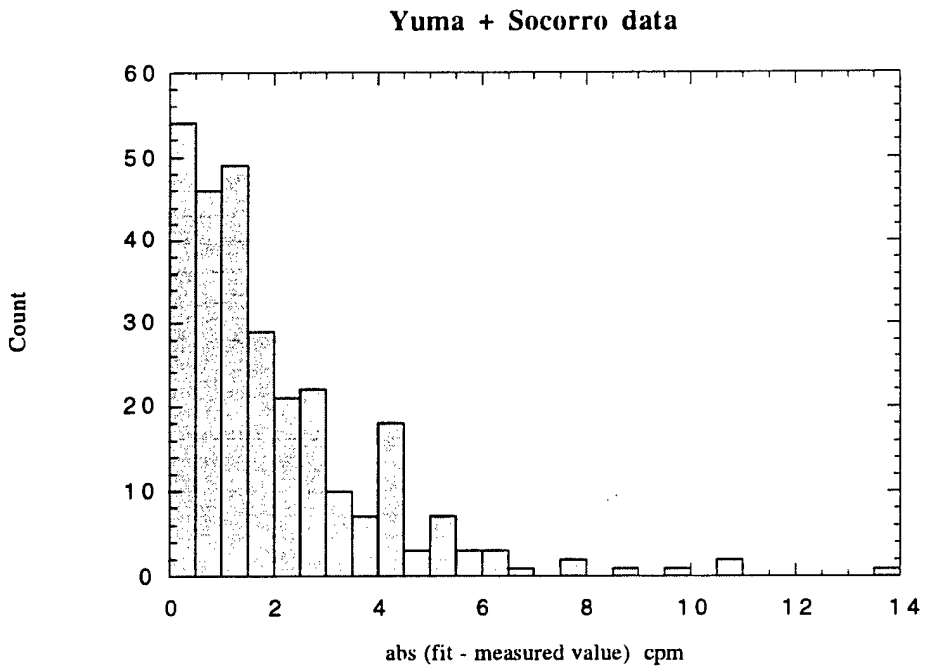

Figure B-1. Combined Data Set

Table B-2. "Goodness of Fit" for Combined Data Set

$\zeta \equiv$ abs (fit – measured signal)	Combined data set (280 total) 1σ = 1.9 cpm
$0 \le \zeta \le 1\sigma$	172
$1\sigma < \zeta \le 2\sigma$	66
$2\sigma < \zeta \le 3\sigma$	30
$3\sigma < \zeta \le 4\sigma$	6
$4\sigma < \zeta \le 5\sigma$	2
$5\sigma < \zeta \le 6\sigma$	3
$6\sigma < \zeta \le 7\sigma$	1

Finally, we present the results obtained if we fit the Socorro data by setting the values of B and β equal to those for the Yuma data and vary only α, because most of the site dependence should manifest itself through α, and the values of B and β should be roughly site independent. We find that the value of α that best minimizes the error defined in Eq. (3.15) in this case is 0.457. The value of the error, however, is 92.57, which is significantly larger than the value obtained by allowing all three parameters to vary. Figure B-2 shows the histogram of the absolute value of the difference between the

measured value and the value predicted for $\alpha = 0.457$, and Table B-3 gives the "goodness of fit." It is clear that this fit is inferior to the original fit to the Socorro data, but it is comparable to that obtained by using all three values of B, α, and β from the fit to the Yuma data. It is somewhat puzzling that the value of α for this fit is larger than that of the Yuma value of 0.322, whereas the value of α for the original fit to the Socorro data was 0.085, a value much less than that for the Yuma data. We can offer no explanation, but we believe that because the original fit to the Socorro data was far superior to this fit, the original fit probably gives a better indication of the true physics of the site.

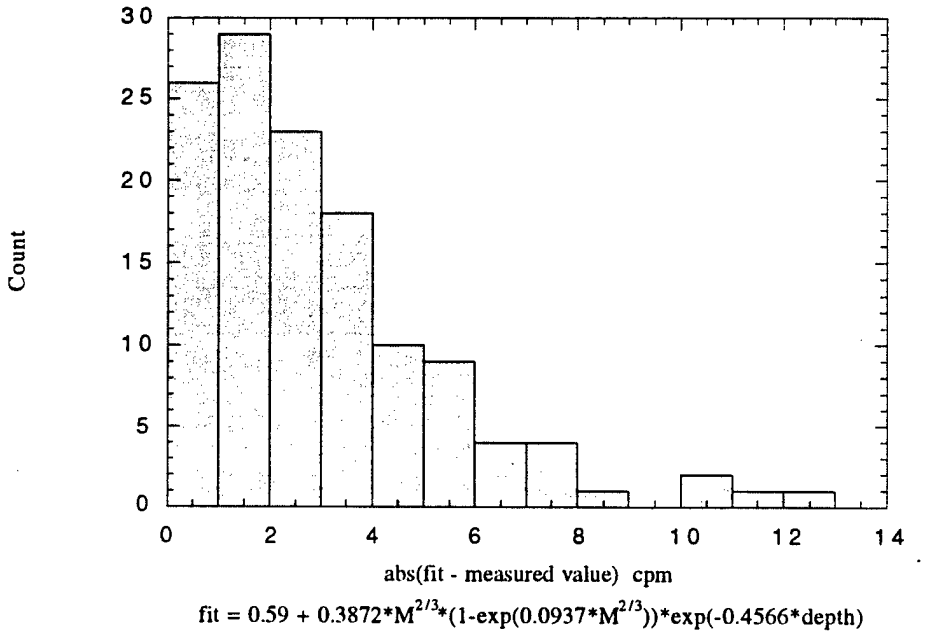

Figure B-2. Socorro Data With B and β Fit to Yuma Values

Table B-3. Goodness of Fits for Socorro Data

$\zeta \equiv$ abs (fit – measured signal) 1σ = 1.5 cpm	Original fit: B = 0.151; α = 0.085 β = 1.826; C = 0.59	Fit to Yuma parameters B = 0.387; α = 0.322 β = 0.094; C = 0.59	Fit B and β to Yuma parameters;optimize α B = 0.387; α = 0.457 β = 0.094; C = 0.59
$0 \le \zeta \le 1\sigma$	74	71	71
$1\sigma < \zeta \le 2\sigma$	40	40	34
$2\sigma < \zeta \le 3\sigma$	10	11	15
$3\sigma < \zeta \le 4\sigma$	2	3	4
$4\sigma < \zeta \le 5\sigma$	2	1	3
$5\sigma < \zeta \le 6\sigma$	–	1	1
$6\sigma < \zeta \le 7\sigma$	—	1	—
error	43.22	104.2	92.57

REPORT DOCUMENTATION PAGE

Form Approved
OMB No. 0704-0188

Public Reporting burden for this collection of information is estimated to average 1 hour per response, including the time for reviewing instructions, searching existing data sources, gathering and maintaining the data needed, and completing and reviewing the collection of information. Send comments regarding this burden estimate or any other aspect of this collection of information, including suggestions for reducing this burden, to Washington Headquarters Services, Directorate for Information Operations and Reports, 1215 Jefferson Davis Highway, Suite 1204, Arlington, VA 22202-4302, and to the Office of Management and Budget, Paperwork Reduction Project (0704-0188) Washington DC 20503

1. AGENCY USE ONLY *(Leave blank)*	2. REPORT DATE	3. REPORT TYPE AND DATES COVERED
	December 1997	Final—October 1996–December 1997

4. TITLE AND SUBTITLE
Assessment of Thermal Neutron Activation Applied to Surface and Near Surface Unexploded Ordnance

5. FUNDING NUMBERS
DASW01 94 C 0054
T-AM2-1528

6. AUTHOR(S)
Lisa Porter, David A. Sparrow

7. PERFORMING ORGANIZATION NAME(S) AND ADDRESS(ES)
Institute for Defense Analyses
1801 N. Beauregard St.
Alexandria, VA 22311-1772

8. PERFORMING ORGANIZATION REPORT NUMBER
IDA Paper P-3339

9. SPONSORING/MONITORING AGENCY NAME(S) AND ADDRESS(ES)
Assistant Deputy Under Secretary of Defense (A&T/Environmental Security)
The Pentagon, Room 3D768
Washington, DC 20301

10. SPONSORING/MONITORING AGENCY REPORT NUMBER

11. SUPPLEMENTARY NOTES

12a. DISTRIBUTION/AVAILABILITY STATEMENT
Approved for public release; distribution unlimited.

12b. DISTRIBUTION CODE

13. ABSTRACT *(Maximum 180 words)*

Thermal neutron activation (TNA) has been proposed for confirming the presence of energetic materials as part of a mine or unexploded ordnance detection system. SAIC, funded through the Night Vision Electro-Sciences Directorate by the Environmental Security Test Certification Program, has carried out proof-of-concept demonstrations of TNA in this confirmatory role at Socorro, NM, and at Yuma, AZ. In this paper, we present a description of the phenomenology of TNA, an analysis of the performance of the SAIC system, and suggestions for hardware upgrades to improve current performance. Our analysis includes the development of a semi-empirical model for the expected signal strength as a function of the target's nitrogen content and depth. We expect this simple model to be useful in future assessments of the feasibility of this approach. We also calculate the P_d/P_{FA} performance of the system at the two sites and determine it to correspond to a signal-to-noise ratio (or figure-of-merit) of order unity. We estimate that an increase in signal-to-noise of roughly 10 will be necessary to make this technology applicable for unexploded ordnance and mine detection. Such order-of-magnitude improvements may be possible if the NaI detectors currently employed are replaced with high purity germanium (HPGe) detectors.

14. SUBJECT TERMS
mine detection, nuclear techniques, neutron techniques, thermal neutron activation, unexploded ordnance

15. NUMBER OF PAGES
66

16. PRICE CODE

17. SECURITY CLASSIFICATION OF REPORT	18. SECURITY CLASSIFICATION OF THIS PAGE	19. SECURITY CLASSIFICATION OF ABSTRACT	20. LIMITATION OF ABSTRACT
UNCLASSIFIED	UNCLASSIFIED	UNCLASSIFIED	SAR